Distinct Regulaton of Bioenergetics and Translation by Gp I mGluRs and NMDARs

Sudhriti Ghosh Dastidar[1,2], Sumita Chakraborty[1], Sumantra Chatterji[1,3], Aditi Bhattacharya[1], Ravi S Muddashetty[1,4,*]

[1]Institute for Stem Cell Biology and Regenerative Medicine,

[2]Manipal Academy of Higher Education,

[3]National Center for Biological Sciences

[4] Lead Contact

* Correspondence: ravism@instem.res.in

Abstract

Neuronal actvity is majorly responsible for dispropotionally large consumption of energy by the brain. However little is known about the nature of the processes responsible for abundant ATP outlay within neurons. Here we provide evidence that major fraction of ATP consumed on glutamate stimulation in cultured cortical neurons is due to activation of global *de-novo* protein synthesis mediated by group I mGluRs. On the contrary NMDAR stimulation leads to a much slower yet protein synthesis dependant ATP expenditure. We found mGluR and NMDAR stimulation impacting the kinetics of translation with distinct kinetics; while mGluR lead to rapid and sustained translation activation as measured by eEF2 phophorylation and matabolic labeling, NMDAR stimulation induced an intial translation inhibition followed by a delayed activation. Translation kinetics for these receptors were always found to have an inverse correlation with Neuronal ATP consumtption. Interestingly, we identified that AMP activated protein kinase (AMPK) has a central role in regulating downstream effects of both mGluR and NMDAR. AMPK activity was reduced on mGluR stimulation even under low ATP levels while there was a rapid increase in AMPK actvity on NMDAR stimulation. Perturbing AMPK function prior to either stimulation led to a complete loss of stimulation specific effects on eEF2 phosphorylation and global translation. Our observation therefore established a pivotal role for AMPK-eEF2 signaling axis on receptor specific regulation of global translation.

43 **Introduction**

44 Brain is known to consume a significant fraction of the body's metabolic energy even
45 at the 'resting' state (1) which increases further on actvity. Evidences from FMRI based
46 studies and PET studies with various tracer molecules have established direct
47 correlations between brain activity and enhanced resource consumption. Conditions
48 such as hypoglycemia and cerebral ischemia leads to severe consequences largely due
49 to perturbations in energy supply (2)(3). Dysregulated energy metabolism is at the heart
50 of conditions such as epilepsy and various neuro-degenerative diseases (4)(5).
51 Therefore, highly regulated energy management is a key requirement for proper
52 cognitive functions of the brain.

53 Synapses are thought to be the sites of major ATP consumption (6)(7) due to large
54 number of cellular processes being activated on arrival of a stimulus. While high rate
55 of endocytosis is reported to consume maximum energy at the pre-synaptic boutons on
56 electrical stimulation (8)(9), our understanding is quite limited as to what extent
57 various processes consume ATP at the post-synaptic compartments and at the pan-
58 neuronal level. Neuronal activity has also been known to induce abundant protein
59 synthesis (10), a determining resource for long term synaptic plasticity and memory
60 formation. Since each round of amino acid incorporation requires 4 ATP molecules along
61 with additional ATP required for amino acid charging and initiation (11)(10), any change
62 therefore in the rate of global protein synthesis is expected to have a reflection on the
63 steady state ATP level. Group I metabotropic glutamate receptors (mGluRs referred
64 hereafter) and NMDARs are widely implicated to facilitate or induce various forms of
65 syanptic plasticity across different brain regions (12)(13). While mGluRs are known to

66 activate translation rapidly (14)(15), NMDAR stimulation causes translation inhibition at
67 an immediate time scale (16). Considering the distinct nature of their downstrem
68 regualtion, it would therefore be interesting to understand the impact of mGluR and
69 NMDAR activation on cellular energetics.

70 Neuronal activity is also known to trigger ATP production through activation of
71 glycolysis and oxidative phosphorylation (8)(17)(18)(19) to support the enhanced
72 consumption. One key molecular player in such a scenario would be AMP activated
73 protein kinase (AMPK). AMPK is a known sensor for cellular ATP/AMP ratio and acts to
74 balance various catabolic and anabolic processes including global translation (20).
75 AMPK activation has been shown to be critical to support synaptic ATP level on neuronal
76 activity (17) and influence various forms synaptic plasticity (21)(22). Thus,
77 understanding how AMPK coordinates activity dependent changes on energetics and
78 translation is of paramount importance. To gain deeper insight at the molecular level
79 of regulation of energy metabolism and translation on neuronal activity, we addressed
80 the following questions: 1) How is the energy level altered over time on synaptic activity
81 2) What are the machanisms that play a key role to dynamically regulate translation on
82 various different stimulations and 3) How AMPK activity is altered to strike a balance
83 between energy and translation regulation.

84 Here we report that stimulation with glutamate, the major neurotransmitter in
85 vertebrate CNS, causes large amount of energy consumption primarily due to the
86 activation of global translation by mGluRs at post synapse and globally throughout the
87 neuron. We also report a distinct difference in the kinetics of translation regulation
88 induced by mGluRs and NMDARs. These distinct responses in turn depend on the

89 differential activation of AMPK downstream of mGluRs and NMDARs involving
90 mechanisms mutually exclusive. Finally, we show that acute prior perturbations of
91 AMPK function lead to complete loss of translation regulation on both stimulations
92 thereby establishing AMPK as biochemical coupling mechanism between energetics and
93 translation on neuronal activity.

94 **Results:**

95 **mGluR dependent protein synthesis consumes significant amount of neuronal ATP**
96 **following glutamate stimulation:**

97 To assess the impact of translation on global ATP levels, we used cultured cortical
98 neurons from Sprague Dawley (SD) rats and stimulated with glutamate (25μM) for 5
99 minutes at day *in vitro* 15 (DIV 15) in presence or absence of protein synthesis inhibitors
100 anisomycin or cycloheximide. We then quantified the ATP/(ATP+ADP) ratio from cell
101 lysates using bioluminescence-based methods (**Figure 1A**). Glutamate Stimulation alone
102 led to significant reduction in the neuronal ATP/(ATP+ADP) ratio. This reduction in the
103 ratio was found to be absent on stimulation in presence of protein synthesis inhibitors
104 anisomycin (25μM) or cycloheximide (100μg/ml) (**Figure 1B**) while drugs alone had no
105 significnat impact. The identical effects of both anisomycin and cycloheximide negates
106 the possibility of off-target effects of these drugs. Thus our observations suggest a large
107 increase in protein synthesis on stimulation, responsible for consuming signifcant
108 fraction of neuronal ATP.

109 Further, to understand the contributions from individual glutamate receptors, we
110 repeated glutamate stimulation inhibiting either ionotropic NMDA and AMPA receptors

111 with a cocktail of D-AP5 (25μM) + CNQX (40μM) (refered to as inotropic glutamate
112 receptor (iGluR) blocker cocktail hereafter) or inhibiting mGluRs with MPEP (10μM). Co-
113 stimulation with iGluR blocker cocktail led to significant reduction in ATP/(ATP+ADP)
114 ratio similar to glutamate alone while stimulation along with MPEP abolished the
115 glutamate mediated reduction significantly (**Figure 1C**). Therefore, these results
116 suggest that the observed reduction in ATP on glutamate stimulation is majorly due to
117 mGluR activity with minimal contributions from the iGluRs. Furthermore, Stimulation
118 in presence iGluR blocker cocktail along with protein synthesis inhibitor anisomycin
119 removed the energy burden significantly (**Figure 1B**) corroborating a robust increase in
120 protein synthesis in absence of iGluR activity consumes significant fraction of neuronal
121 ATP. To further investigate on this idea, we stimulated cortical neurons with mGluR
122 and NMDAR specific agonists s-3,5 DHPG and NMDA (agonists of mGluR and NMDAR
123 respectively). While DHPG treatment led to a significant reduction in ATP/ATP+ADP
124 (79.5±3.8%), NMDA had no significant impact **(Supplementary figure 1A)** ascertaining
125 the importance of mGluR activity on energy consumption. To account for the
126 contribution from endocytosis on glutamate mediated ATP consumption, we blocked
127 GTP dependent enzyme dynamin with small molecule inhibitor dynasore (100μM).
128 Stimulation in presence dynasore had similar effects as that of glutamate alone
129 (**Supplementary figure 1B)** suggesting activity induced vesicle endocytosis has
130 negligible effect on pan-neuronal ATP level.

131 To understand the impact of mGluR and NMDAR stimulation on synaptic energy level,
132 we prepared synaptoneurosomes from whole rat cortices at post-natal day 30 (P30) and
133 stimulated with DHPG (100μM) and NMDA (50μM) respectively (**Figure 1D**).

134 Synaptoneurosome preparation was validated with enrichment of synaptic marker PSD
135 95 without any significant enrichment of glial marker GFAP (**Figure 1E**). Synaptic ATP
136 levels showed significant reduction on mGluR stimulation (**Figure 1F**). The reduction in
137 synaptic ATP levels on stimulation was abolished in presence of mGluR inhibitor MPEP,
138 protein synthesis inhibitor anisomycin and cycloheximide (**Figure 1F**) indicating
139 changes in synaptic ATP level on mGluR stimulation is majorly due to protein synthesis.
140 NMDAR stimulation on the contrary had no significant effect on synaptic ATP level and
141 was unaltered in presence of NMDAR inhibitor D-AP5 (**Figure 1F, supplementary figure**
142 **1C**). Therefore, our observations suggest mGluR dependent protein synthesis creates
143 significant energy demand both at the synaptic and pan-neuronal level.

144 **Figure 1**

145 **Glutamate dependent changes in neuronal ATP/ADP Ratio is primarily due to Group I mGluR**
146 **dependent protein synthesis.**

147 **(A)** Schematic depicting experimental work flow for measurement of ATP/ATP+ADP ratio from
148 cultured cortical neurons at 15 day *in-vitro* (DIV 15) using luciferase-based methods.

149 (**B**) Bar graph representing normalized average value of neuronal ATP/ATP+ADP ratio in
150 unstimulated condition, in presence of Anisomycin (25μM), cycloheximide (350μM), on
151 glutamate (25μM) stimulation alone for 5 minutes, on glutamate stimulation along with
152 anisomycin, on glutamate stimulation along with cycloheximide and on glutamate stimulation
153 in combination with D-AP5, CNQX and anisomycin. Data represented as: mean ± SEM with
154 scattered data points. *$p<0.05$, n=3-6 independent plating. One-way ANOVA followed by
155 Bonferroni's multiple comparison test.

156 (**C**) Bar graph representing normalized average value of neuronal ATP/ATP+ADP ratio in
157 unstimulated condition, in presence of MPEP (10μM), in presence of the cocktail of CNQX (40μM)
158 + D-AP5 (25μM), on glutamate (25μM) stimulation alone for 5 minutes, on glutamate stimulation
159 along with the cocktail of CNQX + D-AP5 and on glutamate stimulation along with MPEP. Data
160 represented as: mean ± SEM with scattered data points. *p<0.05, **p<0.01, ***p<0.001, n=3-5
161 independent plating. One-way ANOVA followed by Bonferroni's multiple comparison test.

162 **(D)** Schematic depicting experimental work flow for measurement of synaptic ATP level from
163 cortical synaptoneurosomes obtained from Sprague dawley rats at post-natal day 30 (P30) using
164 luciferase-based methods.

165 **(E)** Immunoblots showing PSD 95 and GFAP levels on whole cortical lysate and
166 synaptoneurosome preparation. Quantification representing average fold enrichment of PSD 95
167 and GFAP on synaptoneurosome preparations compared to whole cortex lysate.

168 **(F)** Bar graph representing normalized average value of synaptic ATP level in unstimulated
169 condition, on DHPG (100μM) treatment for 5 minutes, on DHPG treatment along with MPEP
170 (10μM), on DHPG treatment along with anisomycin (50μM), on DHPG treatment along with
171 cycloheximide (350μM), on NMDA (40μM) treatment for 5 minutes and on NMDA treatment along
172 with D-AP5 (25μM). Data: mean +/- SEM with scattered data points. *p<0.05, n=5-10
173 independent plating. One-way ANOVA followed by Bonferroni's multiple comparison test.

174 **mGluRs and NMDARs impact synapto-dendritic ATP levels with distinct kinetics**

175 To understand the kinetics of activity induced changes in energy level at a more
176 compartment specific manner, we measured ATP/ADP ratio following mGluR and
177 NMDAR stimulation at the distal dendrites of cortical neurons (~50μm away from cell
178 body) using ratio sensor PercevalHR as reported previously (23) (**Figure 2A**). Perceval

179 pH bias was approximately corrected by simultaneous measurement of intracellular pH
180 with the ratio sensor pH-Red using the linear relation between Perceval and pH-Red
181 fluorescence as described previously (24)(23) **(supplementary figure 2A)**. On bath
182 application of 50μM DHPG (mGluR agonist) we observed a rapid and significant
183 reduction (~ by 2 mins) in the dendritic ATP/ADP ratio. The ratio continued to stay low
184 long as DHPG was present in the media (**Figure 2B-2E**). Application of NMDA (20μM) on
185 bath conversely showed much delayed (~10 minutes post-stimualtion) reduction in the
186 ratio indicating a slow kinetics of NMDAR effect on dendritic ATP:ADP ratio distinctly
187 different to that of mGluRs (**Figure 2B-2E)**. Stimulation in presence of protein synthesis
188 inhibitor anisomycin inhibited the activity dependent reduction in the dendritic
189 ATP/ADP ratio for both DHPG and NMDA treatment (**Figure 2C-2F**). While the dendritic
190 ATP/ADP ratio was unaltered under basal condition, application of anisomycin led to a
191 sharp rise in ATP/ADP ratio reflecting the energy consumption due to basal protein
192 synthesis (**supplementary figure 2B and 2C**). Our observations therefore clearly
193 indicate that stimulation dependent protein synthesis is a major energy burden even at
194 the local dendritic compartments.

195 To investigate the kinetics of ATP regulation at the synapse we used cortical
196 synaptoneurosome preperation. We stimulated synaptoneurosomes for 1, 2 and, 5
197 minutes and allowed recovery for 5 minutes after stimulation (hence reffered to as 5
198 min recovery hereafter). ATP levels were quantified from the specified time points
199 using luminescence-based methods from synaptoneurosomal lysates (**Figure 2F**). DHPG
200 (100μM) addition alone led to a rapid and significant reduction of the synaptic ATP level
201 at 2 minutes and 5 minutes after stimulation and reached baseline at 5 min recovery

202 time point. The DHPG induced changes in synaptic ATP levels was lost in presence of
203 anisomycin highlighting most of the change in the ATP level was contributed by protein
204 synthesis (**Figure 2G**). NMDA stimulation in the same system had no significant impact
205 on the ATP levels till 5 minutes of stimulation but exhibited a significant reduction at
206 5 min recovery time point. Stimulation in presence of anisomycin had no additional
207 effect as that of NMDAR alone (**Figure 2H**) suggesting no detectable amount of protein
208 synthesis happened till 5 minutes of NMDAR stimulation (16). Synaptic ATP level was
209 unaltered in absence of any stimulation for a period similar as stimulations
210 (**supplementary figure 2D**). Together our results indicate mGluR stimulation leads to a
211 rapid and persistent reduction in ATP level in a protein synthesis dependent manner
212 while NMDAR stimulation impacts ATP level with a late onset of protein synthesis.

213 **Figure 2**

214 **mGluR and NMDAR impacts dendritic ATP/ADP ratio with distinct Kinetics.**

215 **(A)** Representative dendrite showing changes on PercevalHR fluorescence ratio (~ATP/ADP
216 ratio) on bath application of DHPG (50μM) and NMDA (20μM). Scale=10μM.

217 **(B)** Average time traces showing the changes in the dendritic ATP/ADP ratio on DHPG and NMDA
218 treatment in presence or absence of anisomycin (25μM). The curved arrow on top indicates the
219 time when stimulants were added and kept in the imaging media. Data: mean +/- SEM, n= 6-8
220 cells from independent plating.

221 **(C)** Bar graph representing average change in PercevalHR fluorescence (ΔF/F) on DHPG
222 treatment, NMDA treatment, DHPG treatment along with anisomycin and NMDA treatment along
223 with anisomycin 2 minutes after stimulant was added on bath. Data: mean +/- SEM. *$p<0.05$,

224 n= 6-8 cells from independent plating. One Way ANOVA followed by Bonferroni's multiple
225 comparison test.

226 **(D)** Bar graph representing average change in PercevalHR fluorescence (ΔF/F) on DHPG
227 treatment, NMDA treatment, DHPG treatment along with anisomycin and NMDA treatment along
228 with anisomycin 5 minutes after stimulant was added on bath. Data: mean +/- SEM. *p<0.05,
229 n= 6-8 cells from independent plating. One Way ANOVA followed by Bonferroni's multiple
230 comparison test.

231 **(E)** Bar graph representing average change in PercevalHR fluorescence (ΔF/F) on DHPG
232 treatment, NMDA treatment, DHPG treatment along with anisomycin and NMDA treatment along
233 with anisomycin 2 minutes after stimulant was added on bath. Data: mean +/- SEM. **p<0.01,
234 n= 6-8 cells from independent plating. One Way ANOVA followed by Bonferroni's multiple
235 comparison test.

236 **(F)** Schematic depicting stimulation protocol in cortical synaptoneurosomes for quantification
237 synaptic ATP levels.

238 **(G)** Line graph showing average synaptic ATP levels at various time points after DHPG (100μM)
239 treatment and 5 minutes after recovery in presence or absence of anisomycin (50μM). Data:
240 mean +/- SEM, *p<0.05, **p<0.01, ****p<0.0001 for comparison with 0 minute. ##p<0.01 and
241 ####p<0.0001 for comparison between DHPG+aniso. n≥ 5 animals per group. Two Way ANOVA
242 followed by Bonferroni's multiple comparison test.

243 **(H)** Line graph showing average synaptic ATP levels at various time points after NMDA (40μM)
244 treatment and 5 minutes after recovery in presence or absence of anisomycin (50μM). Data:
245 mean +/- SEM, **p<0.01 for comparison with 0 minute. n≥ 4 animals per group. Two Way ANOVA
246 followed by Bonferroni's multiple comparison test

247

248 **mGluRs and NMDARs regulate eEF2 phosphorylation to create distinct kinetics of**
249 **translation**

250 To understand the stimulation dependent changes on global translation with a direct
251 correlate, we quantified de-novo protein synthesis at various time points after
252 stimulation using FUNCAT metabolic labeling technique as described previously (25).
253 Cultured cortical neurons (DIV 15) were methionine starved for 1 hour followed by
254 application of methionine analogue AHA and incubation for 1 hour for abundant labeling
255 of proteins. This was followed by stimulation as described in figure 2F and fixation
256 (**Figure 3A**). Newly synthesized proteins were visualized by tagging the AHA containing
257 proteins with Alexa 555 alkyn. Mean FUNCAT intensity was then quantified from somata
258 and dendrites representing quantity of proteins synthesized cumulatively over the
259 period of stimulation (**Figure 3B, 3C, 3D and supplemenatry figure 3B**). On bath
260 application of DHPG, we did not observed any discernable change in the FUNCAT signal
261 by 2 minutes. The signal increased significantly though by 5 minutes and by 5 min
262 recovery as compared to unstimulated cells. This demonstrates a robust and persistent
263 increase in de-novo protein synthesis on mGluR stimulation in cultured cortical neurons
264 (**Figure 3C and 3D**). On the contrary NMDA stimulation led to a significant reduction in
265 FUNCAT signal compared to unstimulated cells by 2 minutes while the signal intensity
266 returned to baseline by 5 minutes of stimulation and continued to stay unchanged till
267 5 min recovery (**Figure 3C and 3D**) indicating a a rapid inhibition of translation on
268 NMDAR stimulation following. No significant change in FUNCAT signal was observed in
269 absence of any stimulation (**supplementary figure 3A**). No detectable signal was

270 observed in absence of any AHA incubation which acted as a negative control for our
271 experiment (**supplementary figure 3A**). Therefore, our observations reveal a robust
272 and persistent activation of translation mediated by mGluRs while NMDAR stimulation
273 led to a rapid inhibition of translation.

274 Eukaryotic elongation factor 2 (eEF2) has been proposed to be a signal integrator (26)
275 and its phosphorylation is known to respond to various synaptic stimuli (16)(27) thereby
276 regulating translation elongation (28). Phosphorylation of Thr 56 residue of eEF2 is
277 known to pause translation elongation thereby causing global translation inhibition (29).
278 To gain insight on the modes of translation regulation downstream of both receptors,
279 we decided to investigate on the role of elongation factor 2 (eEF2) phosphorylation in
280 cultured cortical neurons. We quantified eEF2 phosphorylation 5 minutes after
281 stimulation, a time point corresponding to maximum difference observed in FUNCAT
282 signal (**Figure 3E and Supplementary figure 3C**). We observed a significant reduction
283 in p-eEF2 levels 5 minutes after DHPG treatment as compared to unstimulated cells.
284 NMDA treatment on the contrary robustly increased the p-eEF2 levels in the cell somata
285 and dendrites (**Figure 3F**). Further we used phospho/ total ratio of eEF2 as a readout
286 to gain a snapshot view of global translation in cortical synaptoneurosomes (**Figure 3G**)
287 and in cortical neurons (**supplementary figure 3D**). Synaptoneurosomes were
288 stimulated for different time period as mentioned before (**Figure 2F**). We observed a
289 significant difference in the kinetics of eEF2 phosphorylation regulated by mGluR and
290 NMDAR stimulation (**Figure 3H and supplementary figure 3E**). mGluR stimulation led
291 to an immediate reduction in phospho/total eEF2 ratio by 1 minute. The decrease in
292 the ratio persisted till 5 minutes of stimulation and returned to baseline by 5 mins of

293 recovery. NMDAR stimulation, on the contrary lead to an immediate increase in the
294 phospho/Total eEF2 ratio by 1 minute correlated well with the decrease in FUNCAT
295 signal observed 2 minutes after stimulation in cortical neurons. The increase in the ratio
296 persisted till 5 minutes of NMDAR stimulation and returned to baseline by 5 min recovery
297 time point (**Figure 3H**). The ratio stayed unaltered in absence of any stimulation
298 (**supplementary figure 4B**). Therefore, we found a strong correlation between the
299 global translation and eEF2 phosphorylation downstream of both the glutamate
300 receptor stimulation.

301 **Figure 3:**

302 **mGluR and NMDAR alter global translation by regulating eEF2 phosphorylation with distinct**
303 **kinetics.**

304 **(A)** Schematic depicting the experimental workflow and stimulation protocol to visualize and
305 quantify newly synthesized protein on stimulation through metabolic labeling technique in
306 cortical neurons DIV 15.

307 **(B)** Representative images showing newly synthesized proteins visualized through FUNCAT
308 metabolic labeling (pseudo-colored) in cortical neurons at various time points following DHPG
309 (50μM) and NMDA (20μM) treatment. MAP2B immunolabeling (supplementary figure 3B) was
310 used for identifying neurons and intensity was used for normalization. Scale=10μM.

311 **(C)** Line graph showing average newly synthesized protein intensity before stimulation (basal)
312 and at various time points following DHPG and NMDA treatments. Data: mean +/- SEM,
313 ***$p<0.001$ n= 21-54 neurons per group from 3 independent plating. Two Way ANOVA followed
314 by Bonferroni's multiple comparison test.

315 **(D)** Box plot showing distribution of data points for the newly synthesized protein obtained from
316 various neurons for each group. *p<0.05, **p<0.01, ***p<0.001, ****p<0.0001, n= 21-54 neurons
317 per group from 3 independent plating. One Way ANOVA followed by Bonferroni's multiple
318 comparison test.

319 **(E)** Representative images showing phospho-eEF2 immunolabeling (Pseudo-colored) in cortical
320 neurons on basal, DHPG and NMDA treatments for 5 minutes. MAP2B immunolabeling
321 (supplementary figure 3C) was used for identifying neurons and intensity was used for
322 normalization. Scale=10μM.

323 **(F)** Box plot showing phospho-eEF2 intensity distribution across multiple neurons on basal
324 condition and on DHPG and NMDA treatment for 5 minutes. *p<0.05, **p<0.01, n=31-49 cells per
325 group from 3 independent plating. One-way ANOVA followed by Bonferroni's multiple
326 comparison test.

327 **(G)** Representative immunoblots describing changes in phospho-eEF2 and total-eEF2 levels at
328 various time points after DHPG (100μM) and NMDA (40μM) treatment to cortical
329 synaptoneurosomes. Note in each case phospho and total eEF2 levels were normalized
330 individually to tubulin before calculating the ratio.

331 **(H)** Line graph showing average value for synaptic phospho/total ratio of eEF2 at various time
332 points after DHPG and NMDA treatment and 5 minutes after recovery. Data: mean +/- SEM,
333 **p<0.01, ***p<0.001, ****p<0.0001, n≥ 5 animals per group. Two Way ANOVA followed by
334 Bonferroni's multiple comparison test.

335 **mGluRs and NMDARs regulate AMPK activity in contrasting manner**

336 AMP activated protein kinase (AMPK) is a widely studied global sensor for ATP/AMP or
337 ADP ratio and is known to regulate various catabolic and anabolic processes during

338 energy stress (20). Since mGluRs and NMDARs had contrasting effect on both ATP/ADP
339 ratio and global translation, we sought to understand if AMPK activity was altered to
340 achieve stimulation specific effects. To examine the global status of AMPK activity we
341 quantitated T172 phosphorylation on AMPK α subunit 5 minutes after stimulation in
342 cortical neurons through immunolabeling (DIV 15) (**Figure 4A and supplementary**
343 **figure 4A**). T172 is present in the activation loop of AMPK and its phosphorylation is
344 positively correlated with heightened AMPK activation (30) (Hawley et al., 1996,). We
345 observed a significant decrease in p-AMPK immunolabeling on mGluR stimulation
346 compared unstimulated condition. NMDAR stimulation on the contrary led to a
347 significant rise in the immunolabel indicating an increase in AMPK activity (**Figure 4B**).
348 To understand the temporal changes in AMPK activity, we stimulated cortical
349 synaptoneurosomes with DHPG followed by measurement of phospho/total AMPK ratio
350 (**Figure 4C**). We found a significant decrease in the ratio by about 2 minutes after DHPG
351 treatment persisting till 5 minutes of recovery (**Figure 4D**) while the ratio stayed
352 unaltered in absence of any stimulation (**supplementary figure 4B**). These results
353 indicate that AMPK activity underwent reduction on mGluR stimulation despite an
354 observed decline in the ATP level. Surprisingly, the mGluR mediated reduction in AMPK
355 activity was found to be abolished in presence of anisomycin underscoring the
356 importance of de-novo protein synthesis in regulation of AMPK activity (**Figure 4C and**
357 **4D)**. One pressing idea was therefore to test whether mGluR stimulation leads to
358 synthesis of any protein that would inhibit AMPK phosphorylation. We chose α-SNAP as
359 a potential candidate to investigate, a *cis*-SNARE disassembly factor, reported to act as
360 a phosphatase of AMPK (31). We investigated the α-SNAP protein level on DHPG

361 treatment in cortical synaptoneurosomes (**Figure 4E**). A significant increase in α-SNAP
362 level was observed on 1 min of DHPG addition and was persistent till 5 min recovery
363 (**Figure 4F**), a temporal feature well correlated with AMPK inactivation kinetics (**Figure**
364 **4D**). The DHPG induced increase in α-SNAP level was found to be abolished in presence
365 of protein synthesis inhibitor anisomycin indicating mGluR dependent de-novo synthesis
366 of α-SNAP plays critical role in AMPK dephosphorylation (**Figure 4F**). Further We
367 quantified the association between α-SNAP and AMPK on mGluR stimulation in cortical
368 cultured neurons (**Figure 4G**) as α-SNAP is known to stabilize the de-phosphorylated
369 version of AMPK. We observed a significant increase in colocalization between α-SNAP
370 and AMPK in cortical neurons after DHPG treatment (5 minutes) compared to
371 unstimulated condition (**Figure 4H**). These results therefore suggest a crucial role for
372 protein α-SNAP in mediating mGluR mediated dephosphorylation of AMPK.

373 **Figure 4:**

374 **mGluR inhibit while NMDAR activate AMPK to regulate translation.**

375 **(A)** Representative images showing phospho-AMPK immunolabeling (Pseudo-colored) in cortical
376 neurons on basal, DHPG and NMDA treatments for 5 minutes. MAP2B immunolabeling
377 (supplementary figure 4A) was used for identifying neurons and intensity was used for
378 normalization. Scale=10μM.

379 **(B)** Box plot showing phospho-AMPK intensity distribution across multiple neurons on basal
380 condition and on DHPG and NMDA treatment for 5 minutes. *$p<0.05$, **$p<0.01$, n=30-46 cells per
381 group from 3 independent plating. One-way ANOVA followed by Bonferroni's multiple
382 comparison test.

383 **(C)** Representative immunoblots describing changes in phospho-AMPK and total-AMPK levels at
384 various time points after DHPG (100μM) treatment to cortical synaptoneurosomes in presence
385 or absence of anisomycin (50μM). Note in each case phospho and total AMPK levels were
386 normalized individually to tubulin before calculating the ratio.

387 **(D)** Line graph showing average value for synaptic phospho/total ratio of AMPK at various time
388 points after DHPG treatment and 5 minutes after recovery in presence or absence of
389 anisomycin. Data: mean +/- SEM, *p<0.05, **p<0.01, ****p<0.0001, n= 5 animals per group. Two
390 Way ANOVA followed by Bonferroni's multiple comparison test.

391 **(E)** Representative immunoblots depicting changes in α-SNAP levels at various time points after
392 DHPG treatment to cortical synaptoneurosomes in presence or absence of anisomycin.

393 **(F)** Line graph showing average value for synaptic α-SNAP levels at various time points after
394 DHPG treatment and 5 minutes after recovery in presence or absence of anisomycin. Data:
395 mean +/- SEM. *p<0.05, **p<0.01, n≥ 4 animals per group. Two Way ANOVA followed by
396 Bonferroni's multiple comparison test.

397 **(G)** Representative images showing α-SNAP (green) and AMPK (red) immunolabeling in cortical
398 neurons. Merge shows the colocalization of two channels. Scale=10μM.

399 **(H)** Box plot depicting quantification of co-localization between -SNAP and AMPK in cortical
400 neurons under basal and DHPG treated conditions. **p<0.01, n≥24 cells per group from 3
401 independent plating. Unpaired-sample t test.

402 **NMDAR Regulate AMPK Activity in Ca2+ dependent Manner**

403 We further investigated the kinetics and mechanism of NMDAR mediated AMPK
404 regulation in cortical synaptoneurosomes (**Figure 5A**). We observed a rapid increase in
405 phospho/total AMPK ratio by 1 minute of stimulation and persisting till 5 mins recovery

406 (**Figure 5B**). This observation is in parallel to our previous observation in neurons where
407 NMDA stimulation lead to enhanced phosphorylation of AMPK (**Figure 4B**). Interestingly
408 we did not observe any detectable change in ATP level (**Figure 2I**) at a similar time
409 scale hinting towards an ATP independent regulation of AMPK. CamKIIß, one of the
410 upstream kinases of AMPK (20)(Burkewitz et al. 2014), is known to phosphorylate it in
411 a Ca^{2+} dependent and ATP independent manner. Therefore, we hypothesized that
412 NMDAR dependent increase in AMPK function is mediated by increased cytosolic Ca^{2+}
413 levels entered through open NMDARs. To test the hypothesis, we repeated NMDAR
414 stimulation in absence of extracellular Ca^{2+} (**Figure 5A**). We observed a significantly
415 different AMPK response on NMDA treatment in absence of extracellular Ca^{2+} (**Figure**
416 **5B**). The stimulation dependent increase in phospho/total AMPK ratio was absent in
417 Ca^{2+} free buffer underscoring the importance of Ca^{2+} signaling in this context.
418 Interestingly we observed the NMDA dependent increase in phspho/total eEF2 level was
419 also abolished in absence of extracellular Ca^{2+} (**supplemenatary figure 4D**) clearly
420 demonstrating the importance of Ca^{2+} dependent signaling mechanism in NMDAR
421 dependent translation regulation.

422 We further followed the kinetics of NMDAR mediated Ca^{2+} entry in cortical neurons.
423 Cytosolic free Ca^{2+} level was quantified on NMDAR stimulation using fluorescent based
424 Ca^{2+} probe Fluo-8AM. We observed a rapid increase in Fluo8 fluorescence on NMDA
425 addition and persisted till the presence of stimulant in the media (**Figure 5C, 5F and**
426 **5G**) indicating an increase in intracellular Ca^{2+} on NMDA treatment. The amount of Ca2+
427 entered was non-saturating as could be inferred from further increase in fluorescence
428 on addition of ionomycin in presence of 10mM Ca^{2+} (**Figure 5F**). The observed increase

429 in Ca^{2+} is NMDA specific as pre-treatment with D-AP5 abolished the rise in Ca^{2+} (**Figure**
430 **5D, 5F and 5G**). The Ca^{2+} surge is contributed primarily by synaptic NMDARs as the
431 response was observed to be absent in presence of MK801 (10μM), a compound known
432 to block the open NMDAR channel pores (**supplementary figure 4C; Figure 5G**). The
433 rise in fluorescence on stimulation was abolished in the absence of extracellular Ca^{2+}
434 indicating the source of the ions are majorly extracellular in nature (**Figure 5E, 5F and**
435 **5G**). Therefore, our results indicate NMDAR mediated rapid entry of external Ca^{2+} is
436 responsible for rapid AMPK activation.

437 **Figure 5:**

438 **NMDAR mediated AMPK activation is extracellular calcium dependent.**

439 **(A)** Representative immunoblots describing changes in phospho-AMPK and total-AMPK levels at
440 various time points after NMDA (40μM) treatment to cortical synaptoneurosomes in presence or
441 absence of extracellular Ca^{2+}. Note in each case phospho and total AMPK levels were normalized
442 individually to tubulin before calculating the ratio.

443 **(B)** Line graph showing average value for synaptic phospho/total ratio of AMPK at various time
444 points after NMDA treatment and 5 minutes after recovery in presence or absence of
445 extracellular Ca^{2+}. Data: mean +/- SEM, **$p<0.01$, ****$p<0.0001$, n= 6 animals per group. Two
446 Way ANOVA followed by Bonferroni's multiple comparison test.

447 **(C,D,E)** Representative images depicting intracellular Ca^{2+} levels (Pseudo-colored) of a cortical
448 neuron before stimulation, immediately (15s) after NMDA (20μM) treatment, at a later time
449 point (300sec) after NMDA treatment and after ionomycin treatment along with 10mM Ca^{2+} in
450 presence or absence of extracellular Ca^{2+} and D-AP5. Scale=20μM.

451 **(F)** Representative time trace showing the change in Fluo8 fluorescence on NMDA treatment in
452 presence or absence of extracellular Ca^{2+} and D-AP5. Ionomycin treatment in presence of 10mM
453 Ca^{2+} was used to calculate fluorescence maximum for a particular cell.

454 **(F)** Box plot showing the distribution of $\Delta F/F_0$ across multiple neurons under spontaneously
455 firing condition, on NMDA treatment in presence or absence of Ca^{2+}, on NMDA treatment along
456 with D-AP5 (25μM) and on NMDA treatment along with MK-801. ****$p<0.0001$, $n\geq30$ neurons per
457 group from 3 independent plating. One-way ANOVA followed by Bonferroni's multiple
458 comparison test.

459 **Perturbation of AMPK function disrupts mGluR and NMDAR specific translation**
460 **response**

461 We present two key pieces of experimental evidence to verify the idea that tight
462 regulation of AMPK function is necessary to generate receptor specific translation
463 response. Since mGluR activation lead to inhibition of AMPK function, first we
464 hypothesized that acute activation of AMPK with 5-aminoimidazole-4-carboxamide
465 ribonucleotide (AICAR; 1mM) should preclude the mGluR specific effect on translation.
466 AICAR treatment alone led to significant increase in p-eEF2 levels (**Figure 6B,**
467 **supplementary 5A)** without any significant alteration in FUNCAT signal (**Figure 6D,**
468 **supplementary 5A**) in cortical neurons. These observations establish a direct influence
469 imparted by AMPK on eEF2 phosphorylation and on global translation. Supporting this
470 hypothesis, DHPG mediated reduction in p-eEF2 level was abolished in presence of
471 AICAR (**Figure 6A,B, supplementary figure 5B**) and DHPG induced increase in global
472 translation was absent in presence of AICAR (**Figure 6C,D, supplementary figure 5B**).
473 Next, we examined the impact of AMPK inhition on NMDAR stimulation using AMPK

474 inhibitor Compund C (Dorsomorphin). Blocking AMPK function with Compound C
475 (Dorsomorphin) had no significant impact on basal p-eEF2 level (**6F, supplementary**
476 **5A**) and but led to a significant increase FUNCAT signal (**6H, supplementary 5A**).
477 Interestingly, NMDA application in presence of Compound C completely abolished the
478 NMDA mediated increase in p-eEF2 level (**Figure 6E,F, supplementary figure 5C**) and
479 also diminished the NMDA mediated inhibition of global translation (**Figure 6G,H,**
480 **supplementary figure 5C**). These observations therefore, establish the strong influence
481 of AMPK over receptor mediated translation regulation and highlights the importance
482 of AMPK-eEF2 signaling axis in the same context.

483 **Figure 6:**

484 **Perturbation of AMPK function disrupts receptor specific translation response:**

485 **(A)** Representative images showing phospho-eEF2 immunolabeling (Pseudo-colored) in cortical
486 neurons on basal condition, on DHPG (50μM) treatment for 5 minutes in presence or absence of
487 AICAR (1mM). MAP2B immunolabeling (supplementary figure 5B) was used for identifying
488 neurons and intensity was used for normalization. Scale=10μM.

489 **(B)** Box plot showing phospho-eEF2 intensity distribution across multiple neurons on basal
490 condition, on DHPG treatment for 5 minutes, on AICAR treatment for 1 hour and on DHPG
491 treatment along with AICAR pre-treatment. *$p<0.05$, **$p<0.01$, ****$p<0.0001$, n=17-46 cells per
492 group from 3 independent plating. One-way ANOVA followed by Bonferroni's multiple
493 comparison test.

494 **(C)** Representative images showing newly synthesized proteins visualized through FUNCAT
495 metabolic labeling (pseudo-colored) in cortical neurons under basal condition, on DHPG
496 treatment for 5 minutes in presence or absence of AICAR. MAP2B immunolabeling

497 (supplementary figure 5B) was used for identifying neurons and intensity was used for
498 normalization. Scale=10μM.

499 **(D)** Box plot showing FUNCAT intensity distribution across multiple neurons on basal condition,
500 on DHPG treatment for 5 minutes, on AICAR treatment for 1 hour and on DHPG treatment along
501 with AICAR pre-treatment. ****$p<0.0001$, n=18-57 cells per group from 3 independent plating.
502 Kruskal-Wallis test followed by Dunn's multiple comparison test.

503 **(E)** Representative images showing phospho-eEF2 immunolabeling (Pseudo-colored) in cortical
504 neurons on basal condition, on NMDA (20μM) treatment for 5 minutes in presence or absence of
505 Compound C (10μM). MAP2B immunolabeling (supplementary figure 5B) was used for identifying
506 neurons and intensity was used for normalization. Scale=10μM.

507 **(F)** Box plot showing phospho-eEF2 intensity distribution across multiple neurons on basal
508 condition (Vehicle control), on NMDA treatment for 5 minutes, on Compound C pre-treatment
509 for 1 hour and on NMDA treatment along with Compound C pre-treatment. *$p<0.05$, **$p<0.01$,
510 n=21-36 cells per group from 3 independent plating. Kruskal-Wallis test followed by Dunn's
511 multiple comparison test.

512 **(G)** Representative images showing newly synthesized proteins visualized through FUNCAT
513 metabolic labeling (pseudo-colored) in cortical neurons under basal condition, on NMDA (20μM)
514 treatment for 5 minutes in presence or absence of Compound C (1mM). MAP2B immunolabeling
515 (supplementary figure 5C) was used for identifying neurons and intensity was used for
516 normalization. Scale=10μM.

517 **(H)** Box plot showing FUNCAT intensity distribution across multiple neurons on basal condition,
518 on NMDA treatment for 5 minutes, on Compound C treatment for 1 hour and on NMDA treatment
519 along with Compound C pre-treatment. *$p<0.05$, **$p<0.01$, ****$p<0.0001$, n=24-52 cells per group
520 from 3 independent plating. Kruskal-Wallis test followed by Dunn's multiple comparison test.

521 **(G)** Schematic showing receptor specific regulation of AMPK-eEF2 signaling and their subsequent
522 impact on global translation. mGluR stimulation (Left) have been found to inactivate AMPK
523 necessary for subsequent downregulation of eEF2 phosphorylation. This led to enhanced global
524 *de-novo* translation and consumption of ATP, hence reducing neuronal ATP/ADP ratio. NMDAR
525 stimulation (Right) caused activation of AMPK in extracellular Ca^{2+} dependent manner causing
526 an increase in eEF2 phosphorylation in turn. This leads to inhibition of global translation
527 therefore having no significant alterations in cellular ATP/ADP ratio.

528 **Discussion:**

529 In this work we present multiple lines of evidences showing that activity induced protein
530 synthesis contributes significantly to the energy expenditure in neurons on glutamate
531 stimulation. Our work demostrate that the global de-novo protein synthesis is
532 dynamically regulated by mGluRs and NMDARs with distinct kinetics. As a consequence,
533 we also observed dynamic alterations in energy level with charecteristic temporal
534 features specific to each type of stiumulus. An AMPK-eEF2 signaling nexus combines
535 uniquely to bring about the charecteristic changes in translation with distinct
536 mechanisms for each stimulus.

537 **Protein Synthesis is the major energy consumer on glutamate stimualtion**

538 It was predicted that activity dependent ATP consumption in neurons is largely due to
539 the reversal of ionic fluxes (7). Our study for the first time establishes the significant
540 effect of activity induced protein synthesis on neuronal energy expenditure.
541 Interestingly we failed to observe any noteworthy contribution from vesicle endocytosis
542 at the pan-neuronal ATP level, unlike what has been observed previously in the axon

543 terminals (8). This demonstrates the distinct nature of energy regulations in various
544 compartments as compared to that of the whole neurons.

545 **mGluRs and NMDARs affect rate of global translation differently**

546 We identified distinct roles for mGluRs and NMDARs in glutamate driven energy usage.
547 Our results demonstrates mGluR dependent translation activation consumes significant
548 amount of ATP and shares distinct kinetic features to that of NMDAR. Gp I mGluRs have
549 been widely reported to activate protein synthesis (32)(15) and induce or facilitate
550 long-term depression in excitatory synapses (14) across various brain regions [reviewed
551 in (33)(34)(35)]. Our results indicate that, mGluR mediated translation activation
552 impact global, dendritic and synaptic energy level immediately. Contrarily, NMDAR
553 stimulation accompanies a delayed impact on global, dendritic or synaptic ATP levels
554 through a delayed translation activation as observed previously (16).

555 **The AMPK-eEF2 Signaling to create differential respnse**

556 Our results describe a key role for AMP activated protein Kinase in both mGluR and
557 NMDAR mediated translation regulation. While AMPK is demonstrated to regulate
558 activity induced energy metabolism (17), sustained activity induced GLUT4 membrane
559 expression in nerve terminals (36) and various forms of synaptic plasticity (21)(22), our
560 study provide mechanistic basis coupling its role on regulation of energy metabolism
561 and translation. AMPK is known to influence eEF2 Kinase function either directly (37)
562 or through indirect mechanisms involving inhibition of mTOR-S6K pathway (38), thereby
563 regulating global translation. mGluR mediated inactivation of AMPK can thus also create
564 opportunity for increased mTOR-S6K activity as observed previously (39). These results

565 therefore could explain the dephosphorylation of eEF2 downstream of mGluR
566 stimulation, an effect unexplored previously. The fact that mGluR mediated AMPK
567 activation is protein synthesis depndent led to us investigate the role of AMPK specific
568 phosphatase α-SNAP (31) in this scenario. Increased α-SNAP level and its association
569 with AMPK on mGluR stimulation suggestive of a feedback regulation of AMPK function.
570 NMDAR stimulation on the contrary involved Ca^{2+} dependent activation of AMPK
571 probably involving one of its upstream kinase CamKIIß. This coalates well with the
572 enhanced phosphorylation of eEF2 on NMDA treatment (**supplementary figue 4D**) as
573 observed previously (40).

574 The study also clearly demostrates the importance of protein synthesis in neuronal
575 energy budget particularly during neuronal activity. AMPK plays a pivotal role in
576 dictating this corelation. A deeper elucidation of this corelation would be of greater
577 significance in many patho-physiological conditions such as stroke, epilepsy and
578 neurodegenrerative diseases. Unraveling other signaling mechanisms underlying the
579 connection between protein sysnthesis and energy dynamics and their long term effect
580 on synaptic plasticity may also provide potential theraputic targets for diseases
581 involving impairment in energy metabolism and dysregulated protein synthesis.

582 **Materials and Methods**

583 **Ethics Statement:** All animal work was done in compliance with the procedures
584 approved by the Institutional Animal Ethics committee (IAEC) and the Institutional
585 Biosafety Committee (IBSC), InStem, Bangalore, India. All Work was done with Sprague
586 dawley (SD)rats. Rats were kept in 20-22'c temperature, 50-60 relative humidity, 0.3μm

587 HEPA filtered air supply at 15-20 ACPH and 14/10 light/dark cycle maintained. Food
588 and water were provided *ad libitum*.

589 **Antibodies and Drugs:** Anti-phospho eEF2 antibody (Thr 56; cat no: 2331; Used at
590 1:1000 dilution for western blotting analysis and 1:250 for immunocytochemistry), anti-
591 eEF2 antibody (cat. no 2332; Used at 1:1000 dilution for western blotting analysis),
592 Anti-phospho AMPKα antibody (Thr 172; cat. no: 2535; used at 1:500 dilution for western
593 blotting analysis and 1:100 for immunocytochemistry analysis), anti-AMPK antibody (cat
594 no: 2532; used at 1:1000 dilution for western blotting analysis), Anti-phospho ACC
595 antibody (cat no: 3661; used at 1:1000 dilution for western blotting analysis) were
596 obtained from Cell Signalling Technologies (MA, US). Anti- tubulin antibody (cat no:
597 T9026; used at 1:1000 dilution for western blotting analysis), anti-MAP2B antibody (cat
598 no: M9942; used at 1:500 dilution for immunocytochemistry), anti-rabbit HRP labelled
599 secondary antibody (cat no: A0545 ; used at 1:5000 dilution for western blotting
600 analysis), anti-mouse HRP labelled secondary antibody (cat no: A9044 ; used at 1:5000
601 dilution for western blotting analysis) were obtained from Sigma-Aldrich (St. Louis, MO).
602 Anti-rabbit secondary antibody alexa 555 labelled (cat no: A11032; used at 1:500
603 dilution for immunocytochemistry) and anti-mouse secondary antibody alexa 488
604 labeled (cat no: A11008; used at 1:500 dilution for immunocytochemistry) were
605 obtained from Thermo fisher Scientific (Waltham, MA). Anti-α-SNAP antibody (cat no:
606 X1026; used at 1:1000 dilution for western blotting analysis). Glutamate (25μM), NMDA
607 (20μM for neurons and 40μM for SNS), CNQX (40μM), Anisomycin (25μM for neurons and
608 50μM for synaptoneurosomes), Cycloheximide (100μg/ml), Ouabain octahydrate (1mM),
609 Dynasore hydrate (100μM), Poly-L-Lysine (0.2mg/ml), Pluronic-F-127(0.002%), BAPTA

610 (10mM) and Ionomycin (10μM) were obtained from Sigma-aldrich (St. Louis, MO). S-3,5
611 DHPG (20μM for neurons and 100μM for SNS), 5-aminoimidazole-4-carboxamide
612 ribonucleotide (AICAR, 1mM), D-AP5 (25μM), MK-801 (10μM) and mPEP (10μM) were
613 obtained from Tocris Biosciences. Compound C (dorsomorphin; 40μM in
614 synaptoneurosomes and 20μM in cultured neurons) were obtained from Santa Cruz
615 Biotechnology (Santa Cruz, CA). Fuo-8 AM (2μM) was obtained from AAT Bioquest
616 (Sunnyvale, CA).

617 **Synaptoneurosome preparation** Synaptoneurosomes were prepared from SD WT rat
618 cortices at the age between post-natal day 28-33 (P28-33) following differential
619 centrifugation method as described previously (Hollingsworth et al., 1985 Scheetz,
620 Nairn, & Constantine-paton, 2000 R. S. Muddashetty, Kelic, Gross, Xu, & Bassell, 2007).
621 Briefly, rat cortices were dissected and homogenized at 4°C in 8 volumes of
622 synaptoneurosome (SNS) homogenization buffer [containing (in mM) 25 Tris-HCl pH 7.4,
623 118 NaCl, 4.7 KCl, 1.2 MgSO4, 2.5 CaCl2, 1.53 KH2PO4 and 212.7 glucose, ,
624 supplemented with Complete protease inhibitors (Roche)]. Homogenates were then
625 passed through three 100μm nylon mesh filters followed by one 11μm filter MLCWP 047
626 Millipore (Bedford, MA) and centrifuged at 1000g for 20 minutes at 4°C. The pellet was
627 resuspended into 2ml of the same buffer. In experiments with no Ca^{2+}, $CaCal_2$ was not
628 added in the resuspension buffer. The resuspended SNS particles were then incubated
629 at 37°C to make them metabolically active.

630 **Synaptoneurosome Stimulation:** For Stimulation, synaptoneurosomes were pre-
631 warmed at 37°C for minimum of 5 minutes. A sample fraction aliquoted at this point
632 was considered unstimulated condition or 0 min of stimulation for further analysis. This

633 was followed by Gp I mGluR and NMDAR stimulation with specific agonists (s)3,5-
634 dihydroxyphenylglycine (DHPG; 100μM) and N-methyl D-aspartate (NMDA; 40μM)
635 respectively. Further fractions were collected after 2 minutes and 5 minutes of
636 stimulation. A fraction was collected 5 minutes post-stimulation (5 min stimulation + 5
637 min recovery). For this, the synaptoneurosomes were first stimulated for 5 minutes with
638 agonists. This is followed by removal of the stimulus through centrifugation at 13,000g
639 for 20 seconds and resuspension with 37°C pre-warmed synaptoneurosome
640 homogenization buffer. These synaptoneurosomes were further incubated for 5 minutes
641 and processed for ATP measurement, protein estimation and western blot analysis. For
642 ATP measurements, stimulation was terminated by direct lysis of synaptoneurosomes
643 with equal volume of boiling water (43). This was followed by centrifugation at 20,000g
644 for 2.5 minutes for the measurement of soluble ATP content from the supernatant. For
645 protein estimation and western blot analysis, synaptoneurosomes fractions were
646 centrifuged at 13,000g for 20 seconds followed by lysing with lysis buffer [containing:]
647 (**Stimulation protocol figure 2F**). In experiments involving pre-treatment of drugs, pre-
648 warming period varied depending on the incubation period of various drugs which were
649 directly added after the resuspension step. Untreated control synaptoneurosomes were
650 pre-incubated for same period as drug pre-treatment time for comparisons.

651 **Cell line and primary neuronal culture** Primary neurons were cultured from cerebral
652 cortices as described by Banker & Goslin, 1998. Embryos were obtained from females
653 at the 18th day of gestation period (E18) and cerebral cortices were dissected out in ice
654 cold Hank's balanced salt solution under a dissection microscope. Cells were dissociated
655 with 0.25% trypsin solution at 37°C for 10 minutes followed by mechanical trituration

656 in minimal essential medium (MEM, Thermo fisher) with 10% foetal bovine serum
657 (sigma). Dissociated cells were plated on tissue culture dishes or coverslips coated with
658 poly-L-lysine (0.2 mg/ml in borate buffer, pH 8.5). Neurons were attached to the
659 substrate in MEM with 10% FBS for 3h, followed by defined Neurobasal Medium
660 (Invitrogen) with GlutaMAX™ supplement (Gibco™) and B-27 supplements (Invitrogen)
661 for 14 days at 37°C in a 5% CO_2 environment. For immunocytochemistry, cells plated on
662 coverslips kept in a 10cm diameter tissue culture dish with a plating density of 10^5
663 cells/dish. The coverslips are then inverted onto astroglial bed in neurobasal media
664 after substrate attachment in MEM. For biochemical and immunoblotting experiments,
665 cells were grown on 6 well dishes or 35mm diameter dishes with seeding density
666 $4X10^5$/well. For live imaging experiments, cells were seeded with $2X10^5$/35mm
667 diameter glass bottom dishes.

668 **Metabolic Labelling:** For metabolic labelling of proteins, neurons were incubated for 1
669 hour in methionine-free Dulbecco's Modified Essential Medium (DMEM, Thermo Fisher).
670 This was followed by addition of L-azidohomoalanine (AHA; 1μM) for next 55 minutes in
671 the same medium. At this point a group of cells were fixed with 4% Paraformaldehyde
672 (PFA) for 20 minutes and would be considered as unstimulated basal for further analysis.
673 This was followed by either fixing the cells with 4% PFA or the cells were stimulated
674 with mGluR and NMDAR specific agonists DHPG (50uM) and NMDA (20 uM) respectively
675 for 2 minutes, 5 minutes or post stimulation 5 minutes recovery (5 min stim + 5 min
676 recovery) and subsequently fixed with 4% PFA. Cells were then permeabilized in TBS_{50}
677 [containing (in mM):50 Tris-Base, 150 NaCl] + 0.3% Triton X 100 solution and blocked
678 using TBS_{50} + 0.1% Triton X 100 + 2% BSA + 4% FBS containing blocking solution. Newly

679 synthesized proteins were then labeled with Alexa-Fluor-555–alkyne [Alexa Fluor 488 5-
680 carboxamido-(propargyl), bis (triethylammonium salt)], by allowing the fluorophore
681 alkyne to react with AHA azide group through click chemistry. All reagents were from
682 Thermo Fisher and stoichiometry of reagents were calculated according to the
683 suggested manual by the manufacturer (CLICK-iT cell reaction buffer kit, cat.no.
684 C10269). Signal intensity was then measured using confocal microscopy to calculate the
685 amount of newly synthesized proteins. For specific detection of neuronal cells, MAP2B
686 positive cells were used for analysis.
687 **Immunocytochemistry:** Rat primary cortical neurons were stimulated with either 50μM
688 DHPG or 20μM NMDA for 5mins. Cells were fixed with 4% PFA and processed for imaging
689 as described before. In brief, cells were permeabilized using TBS_{50} + 0.3% T solution and
690 were treated with Tris-Glycine solution (containing in Moles: 0.5 Tris-base and 0.2
691 Glycine) before blocking with blocking buffer [TBS_{50} + 0.1% T) + 2% BSA + 4% FBS].
692 Primary antibodies were incubated in blocking buffer overnight at 4°C under gentle
693 shaking condition followed by washes. Alexa Fluor 488 coupled anti-mouse and Alexa
694 Fluor 555 coupled anti-rabbit secondary antibodies were incubated for 2h at room
695 temperature. Finally, coverslips were mounted for imaging using Mowiol® 4-88
696 mounting media. Images were acquired on a Leica TCS SP5 confocal microscope (Leica
697 Biosystems) with HCX PL APO 63X, NA 1.4, oil immersion objective. Imaging conditions
698 were kept constant across groups. Images were acquired on Olympus FLUOVIEW 3000
699 confocal laser scanning microscope (Olympus Corporation) with HCX PL APO 60x, NA
700 1.4, oil immersion objective. For quantification of fluorescence intensities, images
701 were acquired while keeping the open pinhole configuration to collect lights from

702 planes below and above the focal plane as well. Objective was moved in the Z direction
703 with a step size of 0.5μm for 12 such steps to ensure the light was collected from the
704 entire cell across its thickness. For quantification of colocalization, images were
705 acquired using 2.5x optical zooming of to satisfy Nyquist's sampling theorem of
706 information theory for maximum resolution in the XY direction. Pinhole was kept at 1
707 Airy unit to ensure optimum resolution and confocal stacks were acquired with a step
708 size of 0.3μm calculated based on the fluorophore wavelength. Imaging conditions were
709 kept constant across different data sets, across experiments.

710 **Live Cell fluorescence Microscopy:**

711 **Imaging Dendritic ATP/ADP Ratio:** Cells were imaged on Zeiss LSM 780 confocal laser
712 scanning microscope (Car Zeiss, Oberkochen, Germany) with 63X Zeiss plan-apochromat
713 oil immersion objective, NA 1.4 with argon lasers of specified wavelength. Cells were
714 grown in Neurobasal media containing B27 supplements and Glutamax and were
715 transfected with PercevalHR and pH-Red construct for simultaneous monitoring of
716 intracellular ATP/ADP ratio and pH. pH monitoring was done as suggested in previous
717 studies (45) to correct for the bias created in Perceval HR fluorescence solely due to
718 the change in intracellular pH. Perceval HR was excited with 488/20 nm and 405/20
719 nm band-pass filters and emission was collected through a 520/15nm band-pass filter.
720 Excitation and emission beams were separated through 490 nm short pass dichroic
721 mirror. pH-Red was excited using 561/20nm and 455/10 nm band-pass filters and
722 emission was collected through 630/50 nm band pass filter. A 560 nm short-pass dichroic
723 was used to separate excitation and emission beams.

724 Neurons were imaged at room temperature in 37°C pre-warmed Neurobasal media
725 without phenol red (Thermo Fisher, Waltham, MA, USA) containing 15mM HEPES. For,
726 approximate pH bias removal, the linear relationship established between Perceval HR
727 and pH-Red fluorescence for the high glucose 'ATP Loaded' state by Tantama et. Al.,
728 2014 was used. The relationship was used to predict the pH bias of Perceval HR signal
729 from the continuously monitored pH-Red signal and was normalized to the observed
730 Perceval HR fluorescence for the entire period of experiment. Images were captured at
731 16-bit image format with 512X512 pixel distribution with frame rate of 1 per 15 seconds.
732
733 **Ca^{2+} Imaging:** Growth media from cells grown on glass bottom petri dishes were first
734 removed and were washed with imaging media [containing in mM: 120 NaCl, 3 KCl, 2
735 CaCl2, 1MgCl2, 3 NaHCO3, 1.25 NaH2PO4, 15 HEPES, 30 glucose (pH 7.4). They were
736 then incubated with 2 ml freshly prepared dye solution (2 μM Fluo-8 AM and 0.002%
737 Pluronic F-127 in imaging media) at 37°C for 10 mins followed by a 5 minutes incubation
738 procedure at the same temperature with the imaging media. They were then imaged
739 on Olympus FV3000 confocal laser scanning inverted microscope with 20X air objective
740 lens NA 0.75, illuminated with 488nm solid state lasers. Images were acquired at a rate
741 of single frame per 3.22 sec intervals at room temperature. Cells were imaged for 322
742 sec (100 frames) for recording spontaneous activity, followed by 644 sec (200 frames)
743 with stimulant and 161 sec (50 frames) with KCl (to check neuronal activity) or
744 ionomycin (F_{max}). After background, fluorescence were calibrated to $[Ca^{2+}]_i$ as $[Ca^{2+}]_i$ =
745 389 $(F-F_{min})/(F_{max}-F)$nM. F_{min} was recorded by chelating Ca^{2+} with 10μM ionomycin
746 (Calbiochem) and 10mM BAPTA (Sigma) in independent experiments and F_{max} was
747 recorded by 10μM ionomycin in presence of 2.5mM $CaCl_2$ in each experiment.

748 **Luciferase Assay:** To measure synaptic ATP levels, Cortical synaptoneurosomes were
749 first pre-warmed and then stimulated with Gp I mGluR and NMDAR specific agonists at
750 37°C under constant shaking. Fractions of the stimulated solutions were collected at
751 time points specified before. For treatment with various drugs, the pre-warming period
752 varied depending on the pre-incubation time of the drug before the stimulants were
753 added. Collected fractions were added to equal volume of boiling water to extract the
754 ATP as described previously (Yang et al., 2002). The lysates were then used for
755 quantification of soluble ATP molecules using luciferase based commercial ATP
756 quantification kit (ATP Determination kit, Thermo fisher, Cat.no. A22066) with the help
757 of a standard curve. For measuring ATP/ADP ratio from cortical neurons, cells were
758 stimulated for specified time points and lysed with lysis buffer [containing in mM: 50
759 Tris-Cl (pH-7.4), 150 NaCl, 5 $MgCl_2$, 1% Triton-X-100, supplemented with EDTA free
760 protease inhibitor complex (Sigma, cat. no. S8830) and phosphatase inhibitor cocktail
761 (Roche, ref.no. 04906837001)]. Lysates were then centrifuged at 20,000g for 20 minutes
762 and supernatants were used for measuring ATP using luciferase-based protocol. This
763 was followed by a step converting ADP to ATP which was then used to measure the ATP
764 and ADP level together constituting majority of the adenine nucleotides. This was done
765 using a commercially available luminescence-based kit (ADP/ATP ratio kit, Abcam,
766 cat.no. ab65313) following the user manual suggested by the manufacturer.

767 **Image Analysis:** Image analysis was done using Fiji (ImageJ based image processing
768 package) and IMARIS 9.0 (Bitplane, Oxford instrument company, Belfast, UK) software.
769 For fluorescence intensity quantification, confocal stacks were collapsed using sum
770 slice projection method and mean intensity was quantified from the cells. MAP2B

771 positive cells were used for identification of neurons and quantified mean intensity
772 values were used for normalization. For quantifying co-localization, Pearson's
773 correlation coefficient (PCC) was measured for the cell body and proximal dendrite
774 region (<50μm). For the coefficient analysis, measurement was done after manual
775 thresholding with threshold value of 155 for a 12bit image format. For time frame
776 analysis, mean fluorescence intensity was quantified for the imaged dendritic region
777 from each time frame. Time frame analysis was done using the time series analyser V3
778 plug in from Fiji. Representative images for ratiometric quantifications were generated
779 using the Ratio Plus plug from Fiji where the image was generated by calculating pixel
780 by pixel intensity ratio between two channels.
781 **Statistical Analysis:** Statistical comparisons were done using GraphPad Prism (Prism
782 7.01, Graphpad Software Inc, La Jolla, CA, USA). For group comparisons, the data
783 distributions were first tested for normality using Kolmogorov-Smirnov Goodness-of-Fit
784 Test or Shapiro-Wilk normality test. Depending on the distribution, either parametric
785 or non-parametric tests were used to quantify statistical significance. For groups with
786 <4 data points, the inherent distribution was considered to follow Gaussian distribution
787 unless mentioned. For comparing two groups, Student's t test (two tailed,
788 paired/unpaired) was done to calculate statistical significance. Multiple group
789 comparisons were made using one-way ANOVA followed by Bonferroni's multiple
790 comparison test for parametric distribution and Kruskal-Wallis's Test followed by
791 Dunn's Multiple comparison test. Two-way ANOVA followed by Holm Sidak's multiple
792 comparison test was performed for comapring multiple groups at various time points.

793 Data are presented as mean ± SEM. p values < 0.05 was considered statistically
794 significant.

795 **Acknowledgement**

796 We are thankful to Central Imaging and Flow-cytometry Facility (CIFF) for LSM 780 and
797 FV3000 confocal microscopes, NCBS animal house facility for generously maintingng the
798 rat colony needed for experimentation. We extend our gratitude to Professor M.K.
799 Mathew and Dr. Tina Mukherjee for their helpful comments and discussion. We thanks
800 Chaitra Ananda, Amirthavarshini Devrajan and Sonu. P. Kurien for their gracious efforts
801 in experimental support and data analysis. The work was supported by the Neurostem
802 grant (BT/IN/Denmark/07/RSM/2015-2016) and Center for Brain Development and
803 Repair (CBDR) (BT/MB-CNDS/2013), Department of Biotechnology, Govt. of India. We
804 thank Dr. Garry Yellen, Harvard University for his useful suggestions on PercevalHR
805 experiments.

806 **Author contribution**

807 S.G.D designed and performed the experiments, analyzed data and co-wrote the
808 manuscript. Sumita.C performed Calcium imaging experiments and analyzed data,
809 Sumantra C. provided resources, A.B provided resources and analyzed data, R.M
810 designed experiments and co-wrote manuscripts.

811 **References**

812 1. Mink JW, Blumenschine RJ, Adams DB. Ratio of central nervous system to body
813 metabolism in vertebrates: its constancy and functional basis. Am J Physiol Integr
814 Comp Physiol [Internet]. 1981;241(3):R203–12. Available from:

815 http://www.physiology.org/doi/10.1152/ajpregu.1981.241.3.R203

816 2. Rooijackers HMM, Wiegers EC, Tack CJ, Van Der Graaf M, De Galan BE. Brain
817 glucose metabolism during hypoglycemia in type 1 diabetes: Insights from
818 functional and metabolic neuroimaging studies. Cell Mol Life Sci. 2016;73(4):705–
819 22.

820 3. Schurr A. Lactate, glucose and energy metabolism in the ischemic brain (Review).
821 Int J Mol Med. 2002;10(2):131–6.

822 4. Koenig JB, Dulla CG. Dysregulated Glucose Metabolism as a Therapeutic Target to
823 Reduce Post-traumatic Epilepsy. Front Cell Neurosci [Internet].
824 2018;12(October):350. Available from:
825 http://www.ncbi.nlm.nih.gov/pubmed/30459556%0Ahttp://www.pubmedcentr
826 al.nih.gov/articlerender.fcgi?artid=PMC6232824

827 5. Vallée A, Lecarpentier Y, Guillevin R, Vallée JN. Demyelination in multiple
828 sclerosis: Reprogramming energy metabolism and potential PPARγ agonist
829 treatment approaches. Int J Mol Sci. 2018;19(4).

830 6. Attwell D, Laughlin SB. An energy budget for signaling in the grey matter of the
831 brain. J Cereb Blood Flow Metab. 2001;21(10):1133–45.

832 7. Harris JJ, Jolivet R, Attwell D. Synaptic Energy Use and Supply. Neuron [Internet].
833 2012;75(5):762–77. Available from:
834 http://dx.doi.org/10.1016/j.neuron.2012.08.019

835 8. Rangaraju V, Calloway N, Ryan TA. Activity-driven local ATP synthesis is required

836 for synaptic function. Cell [Internet]. 2014;156(4):825–35. Available from:
837 http://dx.doi.org/10.1016/j.cell.2013.12.042

838 9. Pathak D, Shields LY, Mendelsohn BA, Haddad D, Lin W, Gerencser AA, et al. The
839 role of mitochondrially derived ATP in synaptic vesicle recycling. J Biol Chem.
840 2015;290(37):22325–36.

841 10. Rangaraju V, tom Dieck S, Schuman EM. Local translation in neuronal
842 compartments: how local is local? EMBO Rep [Internet]. 2017;18(5):693–711.
843 Available from:
844 http://embor.embopress.org/lookup/doi/10.15252/embr.201744045

845 11. Schwanhüusser B, Busse D, Li N, Dittmar G, Schuchhardt J, Wolf J, et al. Global
846 quantification of mammalian gene expression control. Nature.
847 2011;473(7347):337–42.

848 12. Hunt DL, Castillo PE. Synaptic plasticity of NMDA receptors: Mechanisms and
849 functional implications. Curr Opin Neurobiol. 2012;22(3):496–508.

850 13. Malenka L. NMDA Receptor-Dependent Long-Term Potentiation and Long-Term
851 Depression (LTP/LTD). 2012;1–16. Available from:
852 https://www.semanticscholar.org/paper/Depression-(-LTP-%2F-LTD-)-NMDA-
853 Receptor-Dependent-Sabatini-
854 Weinberg/17a6e1f48986de2c5553846603b49acf1ce70578

855 14. Huber KM, Kayser MS, Bear MF. Role for Rapid Dendritic Protein Synthesis in
856 Hippocampal Depression. Science (80-). 2000;288(May):1254–6.

857 15. Luchelli L, Thomas MG, Boccaccio GL. Synaptic control of mRNA translation by
858 reversible assembly of XRN1 bodies. J Cell Sci [Internet]. 2015;128(8):1542–54.
859 Available from: http://jcs.biologists.org/cgi/doi/10.1242/jcs.163295

860 16. Scheetz AJ, Nairn AC, Constantine-paton M. NMDA receptor-mediated control of.
861 2000;211–6.

862 17. Marinangeli C, Didier S, Ahmed T, Caillerez R, Domise M, Laloux C, et al. AMP-
863 Activated Protein Kinase Is Essential for the Maintenance of Energy Levels during
864 Synaptic Activation. iScience [Internet]. 2018;9:1–13. Available from:
865 https://linkinghub.elsevier.com/retrieve/pii/S2589004218301652

866 18. Manlio Díaz-García C, Mongeon R, Lahmann C, Koveal D, Zucker H,
867 Correspondence GY, et al. Neuronal Stimulation Triggers Neuronal Glycolysis and
868 Not Lactate Uptake Cell Metabolism Article Neuronal Stimulation Triggers
869 Neuronal Glycolysis and Not Lactate Uptake. Cell Metab [Internet]. 2017;26:361–
870 374.e4. Available from: http://dx.doi.org/10.1016/j.cmet.2017.06.021

871 19. Rangaraju V, Lauterbach M, Schuman EM. Spatially Stable Mitochondrial
872 Compartments Fuel Local Translation during Plasticity. Cell [Internet].
873 2019;176(1–2):73–84.e15. Available from:
874 https://linkinghub.elsevier.com/retrieve/pii/S0092867418316271

875 20. Burkewitz K, Zhang Y, Mair WB. AMPK at the nexus of energetics and aging. Cell
876 Metab [Internet]. 2014;20(1):10–25. Available from:
877 http://dx.doi.org/10.1016/j.cmet.2014.03.002

878 21. Potter WB, O'Riordan KJ, Barnett D, Osting SMK, Wagoner M, Burger C, et al.

879 Metabolic regulation of neuronal plasticity by the energy sensor AMPK. PLoS One.
880 2010;5(2).

881 22. Kong D, Dagon Y, Campbell JN, Guo Y, Yang Z, Yi X, et al. A Postsynaptic
882 AMPK→p21-Activated Kinase Pathway Drives Fasting-Induced Synaptic Plasticity
883 in AgRP Neurons. Neuron. 2016;91(1):25–33.

884 23. Tantama M, Martínez-François JR, Mongeon R, Yellen G. Imaging energy status in
885 live cells with a fluorescent biosensor of the intracellular ATP-to-ADP ratio. Nat
886 Commun. 2013;4(May).

887 24. Pedersen SF, Jørgensen NK, Damgaard I, Schousboe A, Hoffmann EK. Mechanisms
888 of pH(i) regulation studied in individual neurons cultured from mouse cerebral
889 cortex. J Neurosci Res. 1998;51(4):431–41.

890 25. Dieterich DC, Hodas JJL, Gouzer G, Shadrin IY, Ngo JT, Triller A, et al. In situ
891 visualization and dynamics of newly synthesized proteins in rat hippocampal
892 neurons. Nat Neurosci [Internet]. 2010;13(7):897–905. Available from:
893 http://dx.doi.org/10.1038/nn.2580

894 26. Sutton MA, Taylor AM, Ito HT, Pham A, Schuman EM. Postsynaptic Decoding of
895 Neural Activity: eEF2 as a Biochemical Sensor Coupling Miniature Synaptic
896 Transmission to Local Protein Synthesis. Neuron. 2007;55(4):648–61.

897 27. Takei N, Kawamura M, Ishizuka Y, Kakiya N, Inamura N, Namba H, et al. Brain-
898 derived neurotrophic factor enhances the basal rate of protein synthesis by
899 increasing active eukaryotic elongation factor 2 levels and promoting translation
900 elongation in cortical neurons. J Biol Chem. 2009;284(39):26340–8.

901 28. Richter JD, Coller J. Pausing on Polyribosomes: Make Way for Elongation in
902 Translational Control. Cell [Internet]. 2015;163(2):292–300. Available from:
903 http://dx.doi.org/10.1016/j.cell.2015.09.041

904 29. Ryazanov AG, Davydova EK. Mechanism of elongation factor 2 (EF-2) inactivation
905 upon phosphorylation Phosphorylated EF-2 is unable to catalyze translocation.
906 FEBS Lett. 1989;251(1–2):187–90.

907 30. Hawley SA, Davison M, Woods A, Davies SP, Beri RK, Carling D, et al.
908 Characterization of the AMP-activated protein kinase kinase from rat liver and
909 identification of threonine 172 as the major site at which it phosphorylates AMP-
910 activated protein kinase. J Biol Chem. 1996;271(44):27879–87.

911 31. Wang L, Brautigan DL. α-SNAP inhibits AMPK signaling to reduce mitochondrial
912 biogenesis and dephosphorylates Thr172 in AMPKα in vitro. Nat Commun
913 [Internet]. 2013;4:1559. Available from: http://dx.doi.org/10.1038/ncomms2565

914 32. Weiler IJ, Spangler CC, Klintsova AY, Grossman AW, Kim SH, Bertaina-Anglade V,
915 et al. Fragile X mental retardation protein is necessary for neurotransmitter-
916 activated protein translation at synapses. Proc Natl Acad Sci USA [Internet].
917 2004;101(50):17504–9. Available from:
918 http://www.pubmedcentral.nih.gov/articlerender.fcgi?artid=536018&tool=pmc
919 entrez&rendertype=abstract

920 33. Bellone C, Lüscher C, Mameli M. Mechanisms of synaptic depression triggered by
921 metabotropic glutamate receptors. Cell Mol Life Sci. 2008;65(18):2913–23.

922 34. Schulte G. The Class Frizzled Receptors. Pharmacol Rev [Internet].

923 2010;62(4):632–67. Available from:
924 http://pharmrev.aspetjournals.org/content/61/4/395.short

925 35. Jörntell H, Hansel C. Synaptic Memories Upside Down: Bidirectional Plasticity at
926 Cerebellar Parallel Fiber-Purkinje Cell Synapses. Neuron. 2006;52(2):227–38.

927 36. Ashrafi G, Wu Z, Farrell RJ, Ryan TA. GLUT4 Mobilization Supports Energetic
928 Demands of Active Synapses. Neuron. 2017;93(3):606–615.e3.

929 37. Browne GJ, Finn SG, Proud CG. Stimulation of the AMP-activated Protein Kinase
930 Leads to Activation of Eukaryotic Elongation Factor 2 Kinase and to Its
931 Phosphorylation at a Novel Site, Serine 398. J Biol Chem. 2004;279(13):12220–31.

932 38. Inoki K, Zhu T, Guan K-L. TSC2 Mediates Cellular Energy Response to Control Cell
933 Growth and Survival phosphorylation decreases the ability of TSC2 to inhibit the
934 phosphorylation of ribosomal S6 kinase (S6K) and eukaryotic initiation factor 4E
935 binding protein-1 (4EBP1). Cell. 2003;115(5):577–90.

936 39. Hou L. Activation of the Phosphoinositide 3-Kinase-Akt-Mammalian Target of
937 Rapamycin Signaling Pathway Is Required for Metabotropic Glutamate Receptor-
938 Dependent Long-Term Depression. J Neurosci [Internet]. 2004;24(28):6352–61.
939 Available from: http://www.jneurosci.org/cgi/doi/10.1523/JNEUROSCI.0995-
940 04.2004

941 40. Maus M, Torrens Y, Gauchy C, Bretin S, Nairn AC, Glowinski J, et al. 2-
942 Deoxyglucose and NMDA inhibit protein synthesis in neurons and regulate
943 phosphorylation of elongation factor-2 by distinct mechanisms. J Neurochem.
944 2006;96(3):815–24.

945 41. Hollingsworth EB, McNeal ET, Burton JL, Williams RJ, Daly JW, Creveling CR.
946 Biochemical characterization of a filtered synaptoneurosome preparation from
947 guinea pig cerebral cortex: cyclic adenosine 3':5'-monophosphate-generating
948 systems, receptors, and enzymes. J Neurosci [Internet]. 1985;5(8):2240–53.
949 Available from: http://www.ncbi.nlm.nih.gov/pubmed/2991484

950 42. Muddashetty RS, Kelic S, Gross C, Xu M, Bassell GJ. Dysregulated Metabotropic
951 Glutamate Receptor-Dependent Translation of AMPA Receptor and Postsynaptic
952 Density-95 mRNAs at Synapses in a Mouse Model of Fragile X Syndrome. J Neurosci
953 [Internet]. 2007;27(20):5338–48. Available from:
954 http://www.jneurosci.org/cgi/doi/10.1523/JNEUROSCI.0937-07.2007

955 43. Yang NC, Ho WM, Chen YH, Hu ML. A convenient one-step extraction of cellular
956 ATP using boiling water for the luciferin-luciferase assay of ATP. Anal Biochem.
957 2002;306(2):323–7.

958 44. Banker G, Goslin K. Culturing nerve cells. In: Cellular and molecular neuroscience
959 series. 1998. p. 666.

960 45. Tantama M, Yellen G. Imaging changes in the cytosolic ATP-to-ADP ratio
961 [Internet]. 1st ed. Vol. 547, Methods in Enzymology. Elsevier Inc.; 2014. 355-371
962 p. Available from: http://dx.doi.org/10.1016/B978-0-12-801415-8.00017-5

963

964

965

966 ## Supplementary Information

967 **Supplementary Figure 1:**

968 **Quantifying Activity dependent changes in energy level.** (Related to Figure 1)

969 **(A)** Bar graph representing normalized average value of neuronal ATP/ATP+ADP ratio in basal
970 condition and on DHPG (50μM) and NMDA (20μM) treatment for 5 minutes. *$p<0.05$, n=3
971 independent plating. One-way ANOVA followed by Bonferroni's multiple comparison test.

972 **(B)** Bar graph representing normalized average value of neuronal ATP/ATP+ADP ratio in basal
973 condition, on dynasore (100μM) treatment for 30 minutes, on Glutamate (25μM) treatment for
974 5 minutes and on glutamate treatment along with dynaosre pre-treatment. *$p<0.05$, n=3-6
975 independent plating. One-way ANOVA followed by Bonferroni's multiple comparison test.

976 **(C)** Quantification showing the effect of treatment of anisomycin, cycloheximide and MPEP on
977 synaptic ATP level measured from cortical synaptoneurosomes. Data = mean ± SEM with
978 scattered data points.

979 **Supplementary Figure 2:**

980 **Sensor Calibration and Basal ATP measurement.** (Related to Figure 2)

981 **(A)** Graph depicting a linear relationship was established between the percevalHR fluorescence
982 ratio and the pH-Red fluorescence ratio using NH_4Cl pre-pulse method following method
983 established previously (Pederson et. al, 1998, Tantama et. al, 2013). Briefly a gradient of 5-
984 15mM NH_4Cl solution was applied to allow the changes in intracellular pH in a short period of
985 time to avoid any metabolic stress. Changes in PercevalHR fluorescence was measured along
986 with pH-Red fluorescence and the linear relation was used to remove pH bias approximately.

987 **(B)** Representative dendrite showing the temporal profile of PercevalHR fluorescence
988 (ATP/ADP) in unstimulated condition. Scale=10μM.

989 **(C)** Average time traces showing the change in the dendritic ATP/ADP ratio on unstimulated
990 condition in presence or absence of anisomycin. Data= mean ± SEM. n≥3 cells from independent
991 platings per group.

992 **(D)** Quantification showing the changes in synaptic ATP level on unstimulated conditions. Data=
993 mean ± SEM. n= 4 animals.

994 **Supplementary Figure 3:**

995 **Translation Kinetics.** (Related to Figure 3)

996 **(A)** Representative images showing newly synthesized proteins visualized through FUNCAT
997 metabolic labeling (pseudo-colored) in cortical neurons at various time points in unstimulated
998 condition. Absence of AHA while metabolic labeling was used as a negative control. MAP2B
999 immunolabeling (green, inset) was used for identifying neurons and intensity was used for
1000 normalization. The average trace quantification and data point distribution for unstimulated
1001 cells have been presented in Figure 3C and 3D. Scale=10μM.

1002 **(B)** Representative images showing immunolabeling of MAP2B (green) in cortical neurons at
1003 various time points following DHPG and NMDA treatment for the cells used for FUNCAT intensity
1004 quantification. Scale=10μM.

1005 **(C)** Representative images showing immunolabeling of MAP2B (green) in cortical neurons in
1006 basal condition and DHPG and NMDA treatment for 5 minutes for the cells used for p-eEF2
1007 quantification. Scale=10μM.

1008 **(D)** Representative immunoblots describing changes in phospho-eEF2 and total-eEF2 levels at
1009 various time points after DHPG (50μM) and NMDA (20μM) treatment to cultured cortical neurons.

1010 Note in each case phospho and total eEF2 levels were normalized individually to tubulin before
1011 calculating the ratio.

1012 **(E)** Line graph showing average value for neuronal phospho/total ratio of eEF2 at various time
1013 points after DHPG and NMDA treatment and 5 minutes and 10 minutes after recovery. Data:
1014 mean +/- SEM, *p<0.05, **p<0.01, ***p<0.001, n= 3 animals per group. Two Way ANOVA followed
1015 by Bonferroni's multiple comparison test.

1016 **Supplementary Figure 4:**

1017 **Baseline eEF2 phosphorylation and Characterization of NMDAR dependent Ca^{2+} entry.**
1018 (Related to Figure 4 and Figure 5)

1019 **(A)** Representative images showing immunolabeling of MAP2B (green) in cortical neurons in
1020 basal condition and DHPG and NMDA treatment for 5 minutes for the cells used for p-AMPK
1021 quantification. Scale=10μM.

1022 (B) Line graph showing average value for synaptic phospho/total ratio of eEF2 and AMPK at
1023 various time points after DHPG and NMDA treatment and 5 minutes after recovery in cortical
1024 synaptoneurosomes. Data: mean +/- SEM, n≥ 2 animals per group. Two Way ANOVA followed by
1025 Bonferroni's multiple comparison test.

1026 **(C)** Representative images depicting intracellular Ca^{2+} levels (Pseudo-colored) of a cortical
1027 neuron before stimulation, immediately (15s) after NMDA (20μM) treatment, at a later time
1028 point (300sec) after NMDA treatment and after ionomycin treatment along with 10mM Ca^{2+} in
1029 presence MK-801. Scale=20μM.

1030 **(D)** Representative immunoblots describing changes in phospho-eEF2 and total-eEF2 levels at
1031 various time points after NMDA (40μM) treatment to cortical synaptoneurosomes in presence or

1032 absence of extracellular Ca^{2+}. Note in each case phospho and total AMPK levels were normalized
1033 individually to tubulin before calculating the ratio.

1034 **(E)** Line graph showing average value for synaptic phospho/total ratio of eEF2 at various time
1035 points after NMDA treatment and 5 minutes after recovery in presence or absence of Ca^{2+}. Data:
1036 mean +/- SEM, *$p<0.05$, **$p<0.01$, $n \geq 4$ animals per group. Two Way ANOVA followed by
1037 Bonferroni's multiple comparison test.

1038 **Supplementary Figure 5:**

1039 **AMPK perturbations: (related to figure 6)**

1040 **(A)** Representative images showing phospho-eEF2 immunolabeling (Pseudo-colored), newly
1041 synthesized protein through FUNCAT metabolic labeling and MAP2B immunolabeling in cortical
1042 neurons on AICAR (1mM) treatment and Compound C (10μM) treatment for 1 hour. MAP2B
1043 immunolabeling was used for identifying neurons and intensity was used for normalization.
1044 Scale=10μM.

1045 **(B)** Representative images showing immunolabeling of MAP2B (green) in cortical neurons in
1046 basal condition and on DHPG treatment for 5 minutes in presence or absence of AICAR for the
1047 cells used for p-eEF2 and FUNCAT quantification. Scale=10μM.

1048 **(C)** Representative images showing immunolabeling of MAP2B (green) in cortical neurons in
1049 basal condition and on NMDA treatment for 5 minutes in presence or absence of Compound C
1050 for the cells used for p-eEF2 and FUNCAT quantification. Scale=10μM.

1051

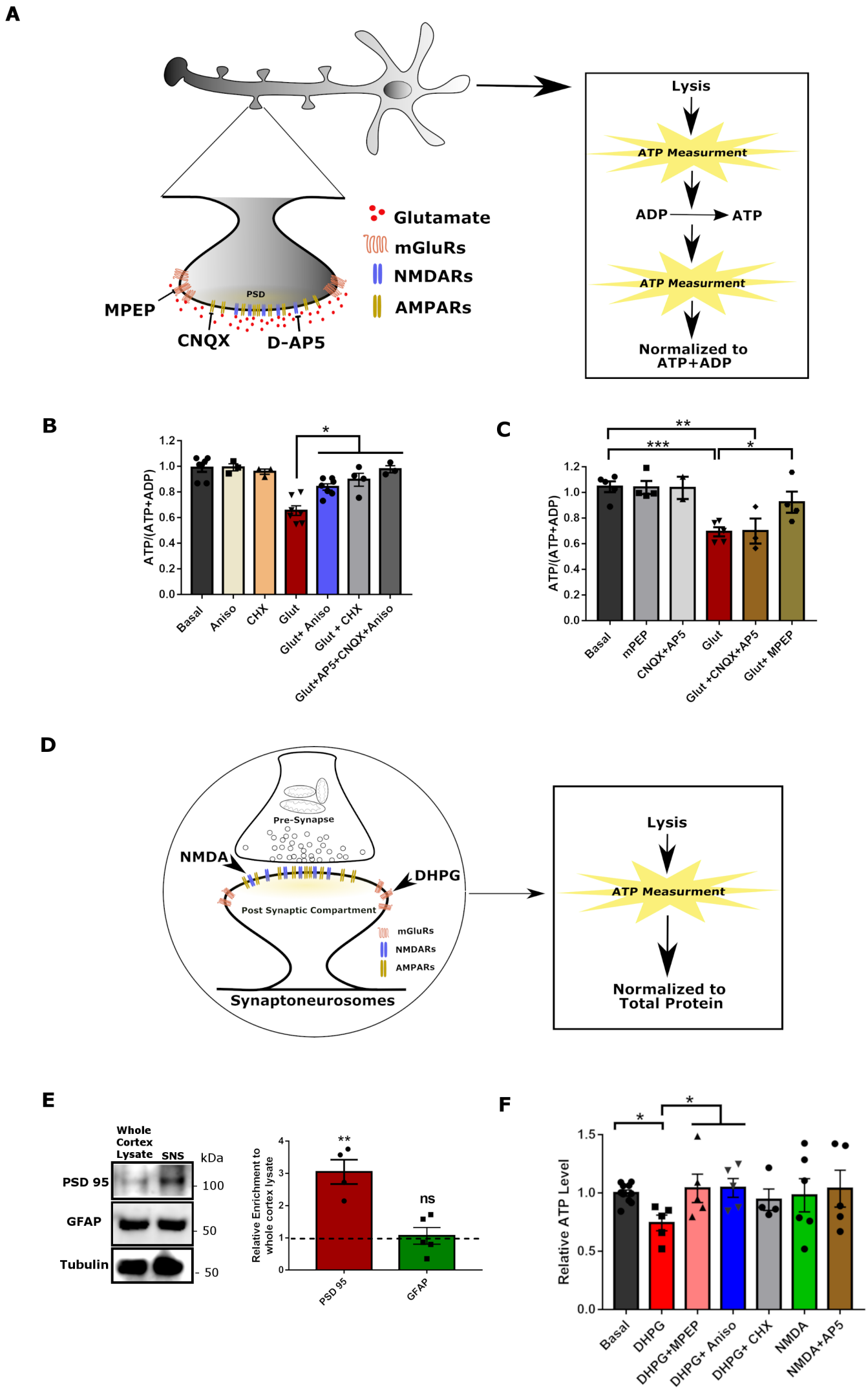
A
Glutamate
mGluRs
NMDARs
AMPARs
PSD
MPEP
CNQX
D-AP5
Lysis
ATP Measurment
ADP
ATP
ATP Measurment
Normalized to ATP+ADP
B
ATP/(ATP+ADP)
Basal
Aniso
CHX
Glut
Glut+ Aniso
Glut + CHX
Glut+AP5+CNQX+Aniso
C
ATP/(ATP+ADP)
Basal
mPEP
CNQX+AP5
Glut
Glut +CNQX+AP5
Glut+ MPEP
D
Pre-Synapse
NMDA
DHPG
Post Synaptic Compartment
mGluRs
NMDARs
AMPARs
Synaptoneurosomes
Lysis
ATP Measurment
Normalized to Total Protein
E
Whole Cortex Lysate
SNS
kDa
PSD 95
GFAP
Tubulin
100
50
50
Relative Enrichment to whole cortex lysate
PSD 95
GFAP
ns
F
Relative ATP Level
Basal
DHPG
DHPG+MPEP
DHPG+ Aniso
DHPG+ CHX
NMDA
NMDA+AP5

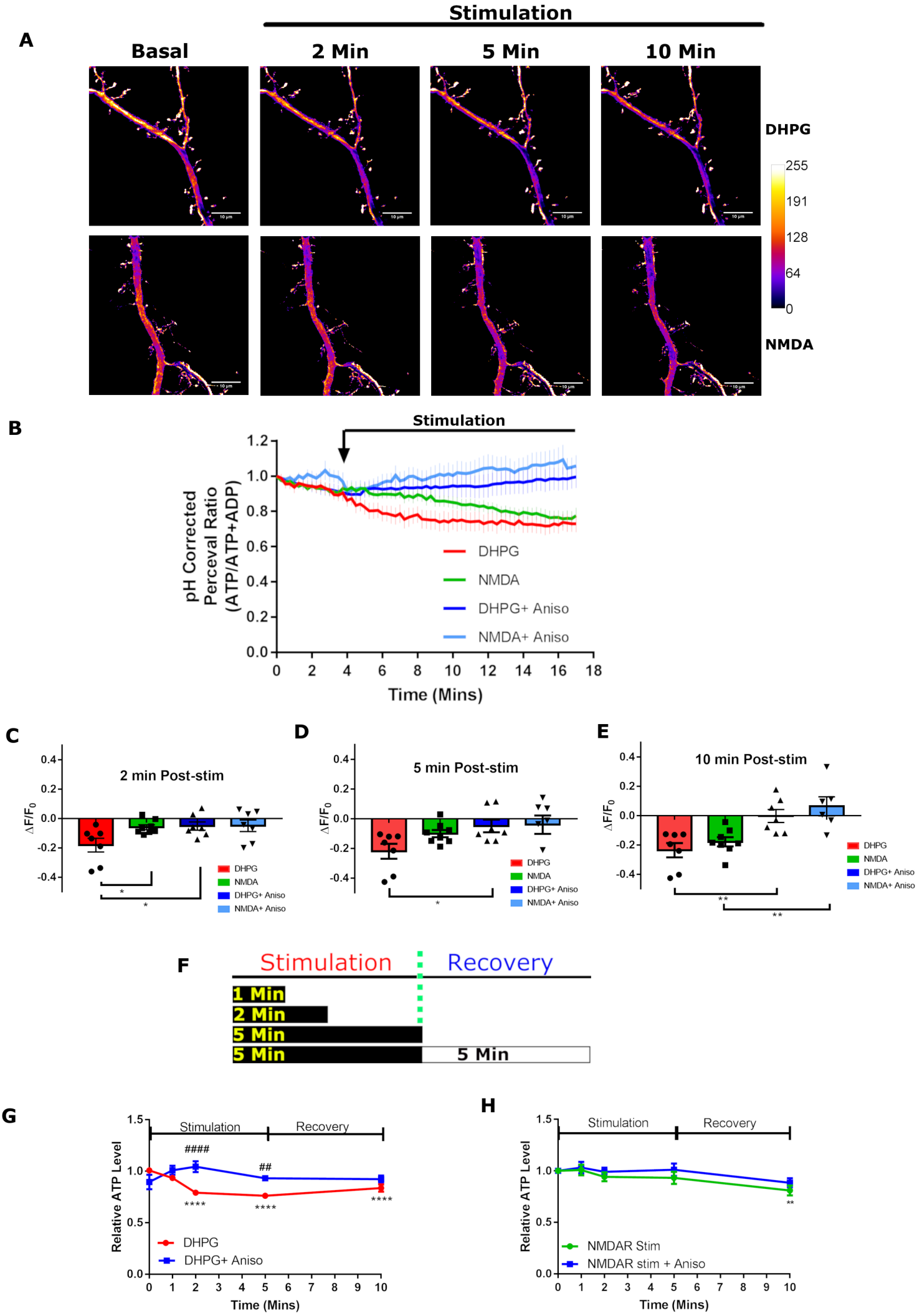
A
Stimulation
Basal
2 Min
5 Min
10 Min
DHPG
255
191
128
64
0
NMDA
B
Stimulation
pH Corrected Perceval Ratio (ATP/ATP+ADP)
DHPG
NMDA
DHPG+ Aniso
NMDA+ Aniso
Time (Mins)
C
2 min Post-stim
D
5 min Post-stim
E
10 min Post-stim
ΔF/F0
F
Stimulation
Recovery
1 Min
2 Min
5 Min
5 Min
5 Min
G
Stimulation
Recovery
Relative ATP Level
DHPG
DHPG+ Aniso
Time (Mins)
H
NMDAR Stim
NMDAR stim + Aniso

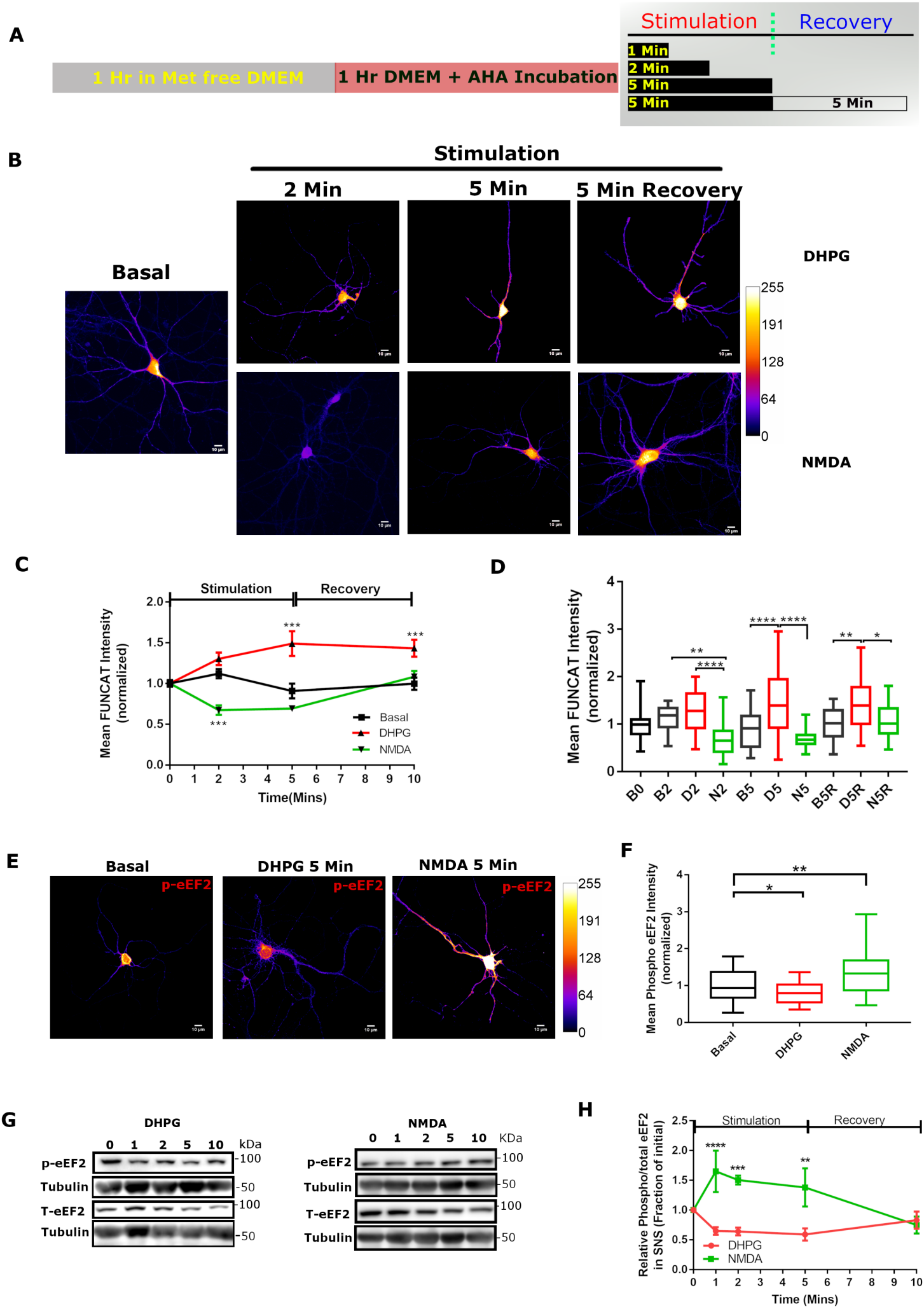
A
1 Hr in Met free DMEM
1 Hr DMEM + AHA Incubation
Stimulation
Recovery
1 Min
2 Min
5 Min
5 Min
5 Min
B
Stimulation
2 Min
5 Min
5 Min Recovery
Basal
DHPG
NMDA
255
191
128
64
0
C
Stimulation
Recovery
Mean FUNCAT Intensity (normalized)
Time(Mins)
Basal
DHPG
NMDA
D
Mean FUNCAT Intensity (normalized)
B0
B2
D2
N2
B5
D5
N5
B5R
D5R
N5R
E
Basal
DHPG 5 Min
NMDA 5 Min
p-eEF2
255
191
128
64
0
F
Mean Phospho eEF2 Intensity (normalized)
Basal
DHPG
NMDA
G
DHPG
0 1 2 5 10 kDa
p-eEF2
Tubulin
T-eEF2
Tubulin
100
50
100
50
NMDA
0 1 2 5 10 KDa
p-eEF2
Tubulin
T-eEF2
Tubulin
100
50
100
50
H
Stimulation
Recovery
Relative Phospho/total eEF2 in SNS (Fraction of initial)
DHPG
NMDA
Time (Mins)

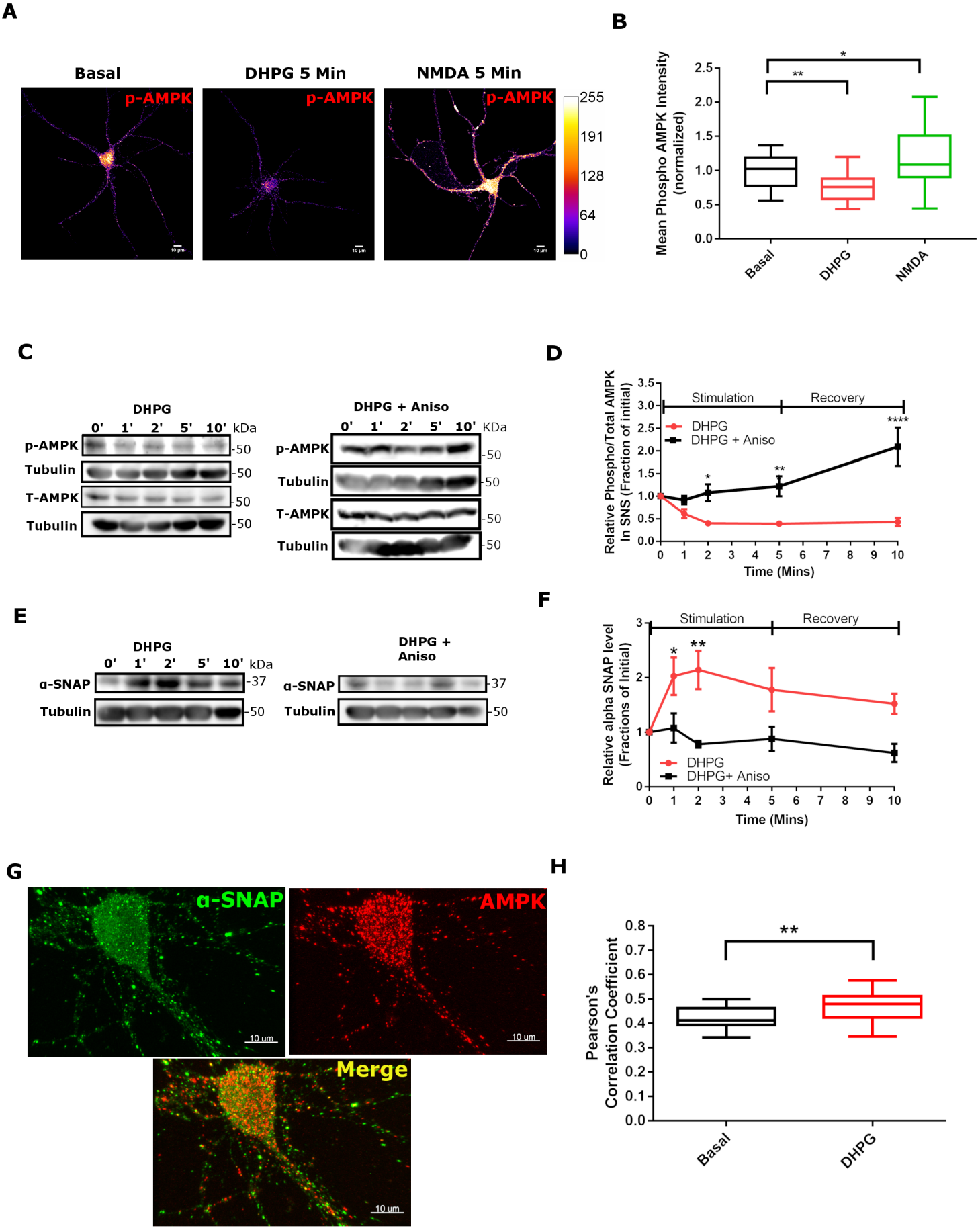
A
Basal
DHPG 5 Min
NMDA 5 Min
p-AMPK
255
191
128
64
0
B
Mean Phospho AMPK Intensity (normalized)
Basal
DHPG
NMDA
C
DHPG
DHPG + Aniso
0' 1' 2' 5' 10' kDa
p-AMPK
Tubulin
T-AMPK
D
Relative Phospho/Total AMPK In SNS (Fraction of initial)
Stimulation
Recovery
DHPG
DHPG + Aniso
Time (Mins)
E
α-SNAP
F
Relative alpha SNAP level (Fractions of Initial)
DHPG+ Aniso
G
AMPK
Merge
10 um
H
Pearson's Correlation Coefficient

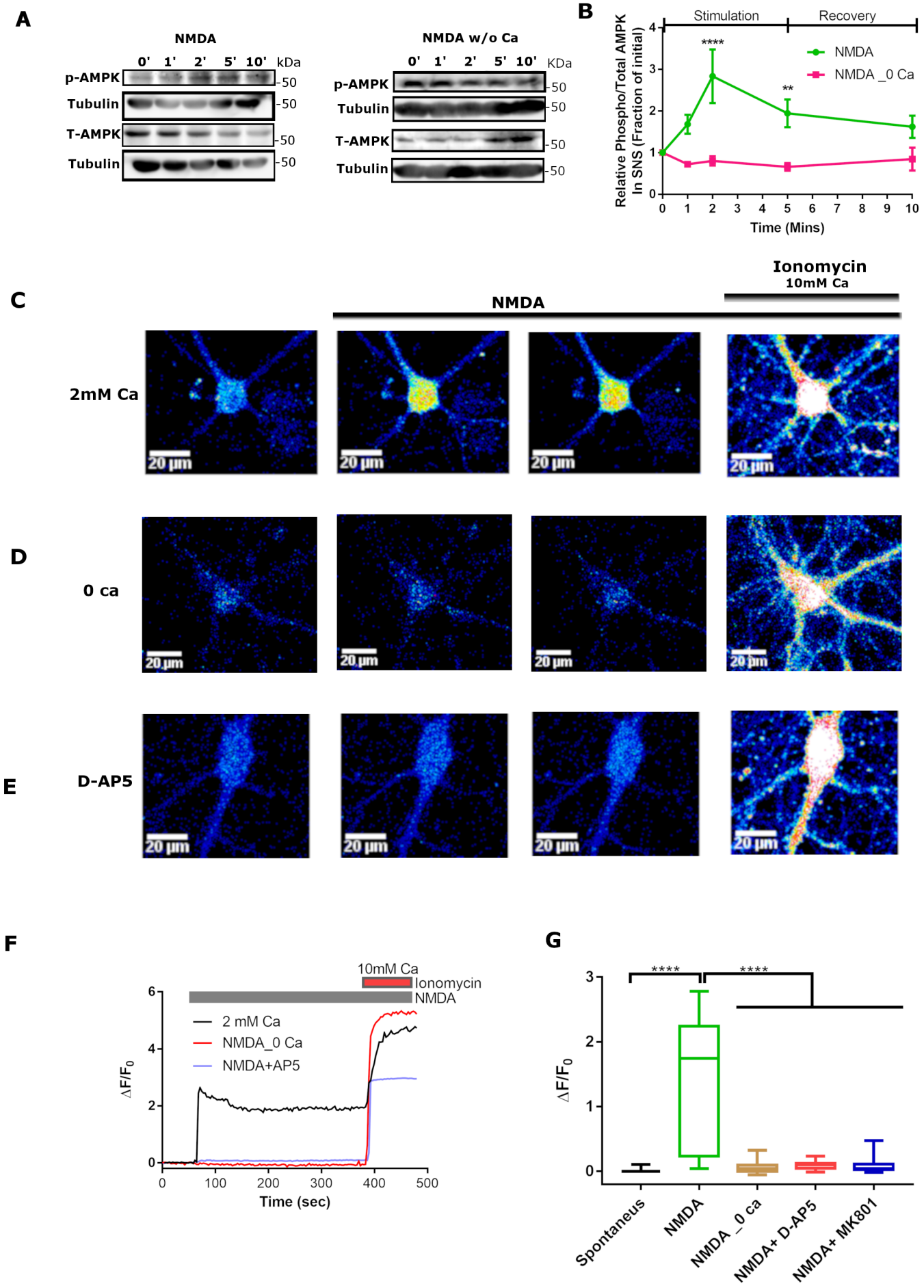
A
NMDA
0' 1' 2' 5' 10' kDa
p-AMPK
Tubulin
T-AMPK
Tubulin
-50
NMDA w/o Ca
B
Stimulation
Recovery
NMDA
NMDA _0 Ca
Relative Phospho/Total AMPK In SNS (Fraction of initial)
Time (Mins)
C
Ionomycin
10mM Ca
NMDA
2mM Ca
D
0 ca
E
D-AP5
20 µm
F
10mM Ca
Ionomycin
NMDA
2 mM Ca
NMDA_0 Ca
NMDA+AP5
ΔF/F0
Time (sec)
G
Spontaneus
NMDA
NMDA _0 ca
NMDA+ D-AP5
NMDA+ MK801

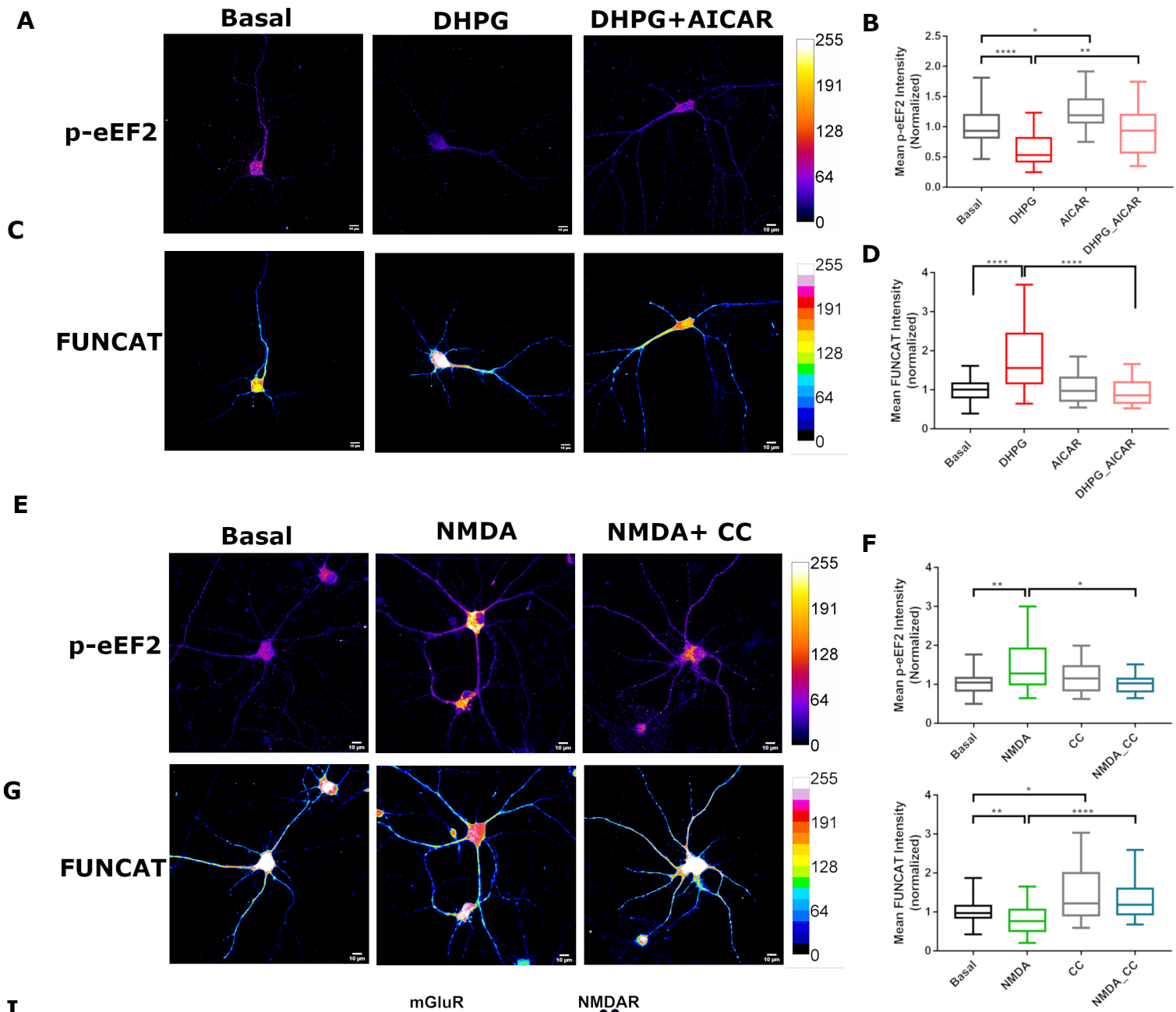
A
Basal
DHPG
DHPG+AICAR
p-eEF2
255
191
128
64
0
B
Mean p-eEF2 Intensity (Normalized)
Basal
DHPG
AICAR
DHPG_AICAR
C
FUNCAT
D
Mean FUNCAT Intensity (normalized)
E
Basal
NMDA
NMDA+ CC
p-eEF2
F
Mean p-eEF2 Intensity (Normalized)
Basal
NMDA
CC
NMDA_CC
G
FUNCAT
Mean FUNCAT Intensity (normalized)

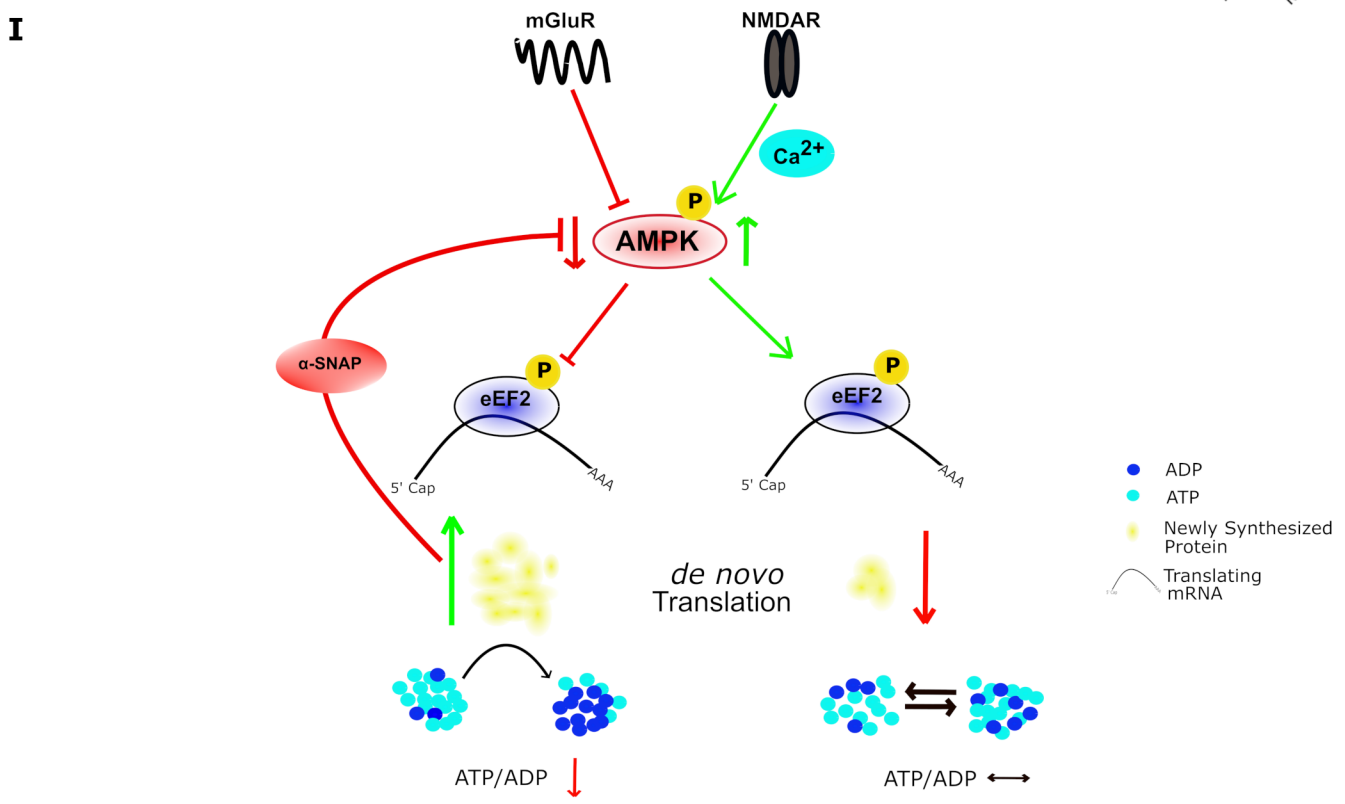
I
mGluR
NMDAR
Ca2+
P
AMPK
α-SNAP
eEF2
5' Cap
AAA
de novo
Translation
ATP/ADP
ADP
ATP
Newly Synthesized Protein
Translating mRNA